Electronic Supplementary Material (ESI) for ChemComm.

Supporting Information

for

Improving Co-Electrocatalytic Carbon Dioxide Reduction by Optimizing the Relative Potentials of Redox Mediatory and Catalyst

Amelia G. Reid, Ethan A. Zelenke, Megan E. Moberg, Diane A. Dickie, and Charles W. Machan*

* - machan@virginia.edu; ORCID 0000-0002-5182-1138

AGR ORCID 0000-0002-2868-4091; EAZ 0009-0008-6855-9907; MEM ORCID 0000-0003-2083-9877; DAD ORCID 0000-0003-0939-3309

Department of Chemistry, University of Virginia,

PO Box 400319, Charlottesville, VA 22904-4319, USA

Table of Contents

Materials and Methods

General

All chemicals and solvents (ACS or HPLC grade) were commercially available and used as received unless otherwise indicated. For all air-sensitive reactions and electrochemical experiments, HPLC-grade solvents were obtained as anhydrous and air-free from a PPT Glass Contour Solvent Purification System. Gas cylinders were obtained from Praxair (Ar as 5.0; CO_2 as 4.0) and passed through activated molecular sieves prior to use. Gas mixing for variable concentration experiments was accomplished using a gas proportioning rotameter from Omega Engineering. UV-vis absorbance spectra were obtained on a Cary 60 from Agilent. An Anton-Parr Multiwave Pro SOLV, NXF-8 microwave reactor was used for microwave syntheses.

Electrochemistry

All electroanalytical experiments were performed using a Metrohm Autolab PGSTAT302N or a Biologic SP-50 potentiostat. Glassy carbon disc working electrodes (⌀ = 3 mm) and non-aqueous silver/silver chloride pseudoreference electrodes behind PTFE tips were obtained from CH Instruments. The pseudoreference electrodes were obtained by depositing chloride on bare silver wire in 10% HCl at oxidizing potentials and stored in a 0.1 M tetrabutylammonium hexafluorophosphate/*N*,*N*-dimethylformamide ($TBAPF_6$/DMF) solution in the dark prior to use. The counter electrode was a glassy carbon rod (⌀ = 3 mm). All CV experiments were performed in a modified scintillation vial (20 mL volume) as a single-chamber cell with a cap modified with ports for all electrodes and a sparging needle. $TBAPF_6$ was purified by recrystallization from ethanol and dried in a vacuum oven before being stored in a desiccator. All data were referenced to an internal ferrocene standard (ferricenium/ferrocene (Fc^+/Fc) reduction potential under stated conditions) unless otherwise specified. All voltammograms were corrected for internal resistance. Ferrocene was purified by sublimation prior to use.

Controlled Potential Electrolysis (CPE)

CPE experiments were performed in a glass Pine Research Instrumentation H-cell with two compartments separated by a glass frit. A 55 mL stock solution of DMF with 0.1 M $TBAPF_6$ was prepared for each bulk electrolysis experiment. Approximately 26 mL of the stock solution was added to each half of the H-cell. One side of the H-cell contained the catalyst, any additional substrate, such as the mediator and/or PhOH, and a glassy carbon rod working electrode. The other side of the H-cell contained approximately 0.075 M ferrocene as a sacrificial reductant along with a graphite rod counter electrode and a Ag/AgCl pseudoreference electrode. The electrolysis experiment was referenced by taking a CV of the side of the H-cell that contained the ferrocene solution. The H-cell was sealed with two septa that were connected by a piece of PTFE tubing which aided to maintain equal pressure between each half of the cell during the electrolysis. Before starting the electrolysis experiment, both sides of the H-cell were sparged with the desired gas for 20 minutes and the sealed cell was allowed to equilibrate for 1 hour. The resistance between the two halves of the H-cell was measured using the i-interrupt procedure available in the NOVA software provided by Metrohm. This measured resistance value was then used to correct for resistance using the iR compensation tool in the NOVA software for potentiostatic experiments.

CPE Product Analysis

During CPE experiments, 250 µL GC injections of the headspace were periodically taken for the detection and quantification of any gaseous products produced. After each CPE experiment, the total volume of solution was measured. The total volume of the sealed H-cell was also measured to account for the total headspace volume for accurate quantification of gaseous products. A calibration curve for CO and H_2 was used to quantify gaseous products produced during electrolysis experiments in the same manner as we previously reported.[1]

Analysis of gas phase products was done by sampling electrolysis headspace through syringe injections into an Agilent 7890B GC equipped with a specialty gas split column 5 Å mol sieve/Porabond Q column (15 m length; 0.320 mm diameter; 25.0 µm film) and thermal conductivity detector with He as a carrier gas. A calibration curve for CO and H_2 was made in the H-cell with an experimental setup containing identical volumes of DMF in 0.1 M $TBAPF_6$ to those used during electrolysis. Known volumes of CO and H_2 were injected into the cell with stirring and 250 µL injections of the headspace were taken for GC injections after equilibration. The limit of detection (LOD) and limit of quantitation (LOQ) for CO and H_2 in the GC were determined from seven consecutive injections at the lowest observable concentrations of each gaseous product respectively. For CO, the LOD was determined to be 5.77 x 10^{-7} moles and the LOQ was determined to be 1.92 x 10^{-6} moles. For H_2, the LOD was determined to be 4.55 x 10^{-6} moles and the LOQ was determined to be 1.52 x 10^{-5} moles.

Calculation of Faradaic Efficiency (FE)

The Faradaic Efficiency (FE) of CO and H_2 was calculated according to the following equation:

$$FE = \frac{N\ x\ n\ x\ F}{Q_{total}} x100\%$$

Where *N* is the moles of product (either CO or H_2), *n* is the number of electrons in the catalytic reaction (*n*=2 for both CO and H_2), *F* is Faraday's constant (96485 C/mol) and Q_{total} is the total charge (C) passed during the CPE experiment.

Calculation of Overpotential for CO_2 Reduction with PhOH Present (Adapted)

The calculation of overpotential for all catalysts was performed according to reported methods.[2] The following equation was used for the determination of the reaction standard potential in V with respect to the Fc^+/Fc couple:

$$E_{CO2/CO} = -0.73\ V - 0.059(pK_a) \qquad \textbf{Eq (1)}$$

The pK_a for PhOH in DMF is reported as 18.8:[3]

$$E_{CO2/CO}(PhOH) = -1.84\ V\ vs\ Fc^+/Fc \qquad \textbf{Eq (2)}$$

The $E_{cat/2}$ determined experimentally for Cr(^{tbu}dh^{Ph}phen)Cl(H_2O), Cr(^{tbu}dhphen)Cl(H_2O), and Cr(^{tbu}dh^{tbu}bpy)Cl(H_2O) is –1.93 V, –1.96 V[4], and –2.00 V[5] vs Fc^+/Fc, respectively. For protic CO_2 reduction (1.0 mM catalyst and 0.1 M PhOH under CO_2 saturation); the overpotential is:

$$\eta = \left|E_{cat/2} - E_{CO2/CO}\right| \qquad \textbf{Eq (3)}$$

Cr(^{tbu}dh^{Ph}phen)Cl(H_2O) **1** η = 90 mV

Cr(^{tbu}dhphen)Cl(H_2O) **2** η = 120 mV
Cr(^{tbu}dh^{tbu}bpy)Cl(H_2O) **3** η = 160 mV

This assumes no contribution from homoconjugation of the acid. We note that the homoconjugation constant (HA_2^-) for PhOH in DMF has been reported as $\log(K_{HA_2^-})$ = 3.8.[6] Therefore, we emphasize that the described overpotential calculated above for PhOH is the lower-limit approximation, as homoconjugation is expected to alter the effective overpotential. The overpotential equation can be modified to account for homoconjugation:

$$E_{CO2/CO} = -0.73\ V - 0.059(pK_a) - \frac{-2.303RT}{nF}\log\left(mK_{HA_2^-}\right) \qquad \textbf{Eq (4)}$$

Where n = number of electrons (2) and m = number of proton transfers (2). The modified equation provides $E^0_{CO2/CO}$ = −1.72 V and the following η values:

Cr(^{tbu}dh^{Ph}phen)Cl(H_2O) **1** η = 210 mV
Cr(^{tbu}dhphen)Cl(H_2O) **2** η = 240 mV
Cr(^{tbu}dh^{tbu}bpy)Cl(H_2O) **3** η = 280 mV

This value does not account for the possible thermodynamic contributions of the water coordinated to the pre-catalyst, the equimolar quantities of water produced for each equivalent of CO generated, or any adventitious H_2O present in the CO_2, solvent, or electrolyte. Under CO_2 saturation, any water present can form carbonic acid, pK_a(DMF) 7.37,[7] and generate new equilibria involving CO_2 and bicarbonate. The role of carbonic acid (and the general hydration of CO_2 in non-aqueous solvent systems) in altering the overall thermodynamics combined with the effects of homoconjugation has been assessed by Matsubara.[8] Considering the role of water, Matsubara obtained a standard potential for CO_2 reduction to CO of −1.70 V versus Fc^+/Fc for PhOH in *N,N*-DMF with 10 mM water present (see below). Note the same value is obtained considering 10 mM water only.

For 10 mM H_2O in DMF, where AH = PhOH:[8]

$$3CO_{2(g)} + H_2O_{(sol,x)} + 2e^- \rightleftharpoons CO_{(g)} + 2HCO_{3\,(sol)}^- \qquad E^0 = -1.70\ V\ vs.Fc^+/Fc$$
$$CO_{2(g)} + 2AH_{(sol)} + 2e^- \rightleftharpoons CO_{(g)} + 2A^-{}_{(sol)} + H_2O_{(sol,x)} \qquad E^0 = -1.96\ V\ vs.Fc^+/Fc$$
$$CO_{2(g)} + 4AH_{(sol)} + 2e^- \rightleftharpoons CO_{(g)} + 2HA_{2\,(sol)}^- + H_2O_{(sol,x)} \qquad E^0 = -1.70\ V\ vs.Fc^+/Fc$$

Determination of TOF from Preparative Electrolysis

The integrated expression of current for a homogeneous electrocatalytic response (considering an application of steady-state conditions to the substrate) has been solved previously:[9, 10]

$$\frac{i}{FA} = \frac{n_{cat}^{\sigma}[cat]\sqrt{(k_{obs}D_{cat})}}{1 + \exp\left[\frac{F}{RT}\left(E_{app} - E_{1/2}\right)\right]} \text{where}$$
$$\frac{i}{A} = J = CO\ specific\ current\ density$$

Substituting and rearranging the first expression to solve for k_{obs}

$$k_{obs} = \frac{J^2\left(1 + \exp\left[\frac{F}{RT}\left(E_{app} - E_{1/2}\right)\right]\right)^2}{F^2(n_{cat}^{\sigma}[cat])^2 D_{cat}}$$

with k_{obs} in hand, the TOF can be expressed for a given potential according to the following relationship

$$TOF = \frac{k_{obs}}{1 + \exp\left[\frac{F}{RT}\left(E_{app} - E_{1/2}\right)\right]}$$

Parameters for CPE experiments reported here not found in **Table 1**.

- $E_{1/2}$ catalyst:
  - −1.93 V vs Fc^+/Fc for Cr(^{tbu}dh^{Ph}phen)Cl(H_2O) **1**
  - −1.96 V vs Fc^+/Fc for Cr(^{tbu}dhphen)Cl(H_2O) **2**
  - –2.00 V vs Fc^+/Fc for Cr(^{tbu}dh^{tbu}bpy)Cl(H_2O) **3**
- Temperature: 298.15 K
- $[CO_2]$: 2.3 x 10^{-4} mol cm^{-3}
- Diffusion coefficient:
  - 2.21 x 10^{-6} cm^2 s^{-1} for Cr(^{tbu}dh^{Ph}phen)Cl(H_2O) **1**
  - 1.60 x 10^{-6} cm^2 s^{-1} for Cr(^{tbu}dhphen)Cl(H_2O) **2**[4]
  - 2.18 x 10^{-6} cm^2 s^{-1} for Cr(^{tbu}dh^{tbu}bpy)Cl(H_2O) **3**[5]
- Electrode area: 3.65 cm^2 or 2.48 cm^2

Calculation of Diffusion Coefficient

The calculation of the diffusion coefficient for the Cr(^{tbu}dh^{Ph}phen)Cl(H_2O) **1** catalyst was performed by reported methods.[12] Cyclic voltammetry (CV) experiments were done with a solution of 1.0 mM catalyst in 0.1 M $TBAPF_6$/DMF under Ar saturation conditions. The scan rate of these CVs was varied from 25 mV/s to 5000 mV/s (**Figure S7**). The increase in current observed as the scan rate increases can be represented by the following equation where i_p is the peak current, n is the number of electrons, A is the area of the electrode, D is the diffusion coefficient, C is the concentration of analyte, and v is the scan rate:

$$i_p = (2.69 \times 10^5) n^{3/2} A C D^{1/2} v^{1/2}$$

By plotting the current density as a function of $v^{1/2}$ for the reversible reduction (**Figure S7**), the slope can be used to find D for each molecule.

$$D_{cat} = \frac{(\text{slope})^2}{n^3 C^2 (2.69 \times 10^5)^2}$$

Calculation of Active Species at a Given Potential

The calculation of the percent of Cr(^{tbu}dh^{tbu}bpy)Cl(H_2O) **3** reduced at a given potential can be achieved by rearranging the Nernst equation where E is the experimental potential (–1.96 V), E^0 is the standard reduction potential of the catalyst (–2.00 V), R is the ideal gas constant (Joule mol^{-1} K^{-1}), T is the temperature (K), n is the number of electrons, F is Faraday's constant (96485 C mol^{-1}), $[A]$ is the concentration of catalyst, and $[B]$ is the concentration of reduced catalyst:

$$E = E^0 - 2.303\frac{RT}{nF}\log_{10}\left(\frac{[B]}{[A]}\right)$$

$$E^0 - E = 2.303\frac{RT}{nF}\log_{10}\left(\frac{[B]}{[A]}\right)$$

$$\frac{E^0 - E}{2.303\frac{RT}{nF}} = \log_{10}\left(\frac{[B]}{[A]}\right)$$

$$\frac{E^0 - E}{2.303\frac{RT}{nF}} = \log_{10}\left(\frac{[B]}{[A]}\right)$$

$$10^{\frac{E^0 - E}{2.303\frac{RT}{nF}}} = \frac{[B]}{[A]}$$

$$if\ \frac{[B]}{[A]} = 0.211, then\ \frac{[B]}{[A]} = \frac{211}{1000}$$

$$and\ \%[B]\ in\ solution = \frac{211}{1211} \bullet 100 = 17.4\%$$

Single Crystal X-ray Diffraction

A single crystal of BNTD was coated with Paratone oil and mounted on a MiTeGen MicroLoop. The X-ray intensity data were measured on a Bruker D8 Venture Kappa four-circle diffractometer system equipped with an Incoatec IμS 3.0 micro-focus sealed X-ray tube (Mo Kα, λ = 0.71073 Å) and a HELIOS double bounce multilayer mirror monochromator. The frames were integrated with the Bruker SAINT software package[13] using a narrow-frame algorithm. Data were corrected for absorption effects using the Multi-Scan method (SADABS).[14] The structure was solved and refined using the Bruker SHELXTL Software Package[15] within APEX5[13] and OLEX2.[16] Non-hydrogen atoms were refined anisotropically. Hydrogen atoms were placed in geometrically calculated positions and were refined isotropically with U_{iso} = 1.2U_{equiv} of the parent atom.

Table S1. Crystallographic data for BNTD

	BNTD
CCDC number	2350924
Formula	$C_{16}H_{10}O_2S$
FW (g/mol)	266.30
Temp (K)	100(2)
λ (Å)	0.71073
Size (mm)	0.081 x 0.127 x 0.158
Crystal habit	yellow plate
Crystal system	triclinic
Space group	P -1
a (Å)	7.6112(4)
b(Å)	8.5345(5)
c (Å)	9.9571(6)
α (°)	111.229(2)
β (°)	102.154(2)
γ (°)	93.290(2)
Volume (Å^3)	583.02(6)
Z	2
Density (g/cm^3)	1.517
μ (mm^{-1})	0.270
F(000)	276
θ range (°)	2.27 to 27.48
Index ranges	-8 ≤ h ≤ 9 -11 ≤ k ≤ 11 -12 ≤ l ≤ 12
Data / restraints /parameters	2657 / 0 / 172
GOF on F^2	1.075
R_1 (I>2σ(I))	0.0399
wR_2 (all data)	0.1089

Synthesis and Characterization

Synthesis of 6,6'-Di(3,5-di-*tert*-butyl-2-hydroxybenzene)-4,7-di-phenyl-1,10-phenanthroline, $^{tbu}dh^{Ph}phen(H)_2$

The synthesis of the 2,9-dichloro-4,7-diphenyl-1,10-phenanthroline starting material was adapted from a previously reported procedure[17] using a 4,7-diphenyl-1,10-phenenthroline starting material. The (3,5-di-*tert*-butyl-2-hydroxy-phenyl)boronic acid starting material was synthesized as previously reported.[1]

A microwave tube was charged with 2,9-dichloro-4,7-diphenyl-1,10-phenanthroline (0.500 g, 1.25 mmol), (3,5-di-*tert*-butyl-2-hydroxy-phenyl)boronic acid (0.935 g, 3.74 mmol), sodium carbonate (0.924 g, 8.72 mmol), $Pd(PPh_3)_4$ (0.072 g, 0.062 mmol), degassed toluene (30 mL), water (12 mL), and methanol (8 mL). The microwave conditions were set to heat the reaction mixture to 170 °C as fast as possible and then held at that temperature for 200 minutes. After the reaction cooled, the reaction layers were separated. The organic layer was extracted with brine (1 x 50 mL) and the aqueous layer was extracted with dichloromethane (3 x 50 mL). All organic fractions were combined and dried over $MgSO_4$ before removing the solvent via reduced pressure leaving an orange solid. Methanol was added to the flask and the mixture was filtered leaving a bright orange solid with an isolated yield of 39.2% (0.362 g). ^{1}H NMR (CD_2Cl_2, 600 MHz): δ 14.69 (s, 2H, O*H*), 8.23 (s, 2H, Ar*H*), 7.88 (d, 2H, Ar*H*), 7.82 (s, 2H, Ar*H*), 7.59 (m, 10 H, Ar*H*), 7.53 (d, 2H, Ar*H*), 1.58 (s, 18H, −C(CH_3)$_3$), 1.40 (s, 18H, −C(CH_3)$_3$). ^{13}C{^{1}H} NMR (CD_2Cl_2, 100 MHz): δ 159.4 (Ar*C*), 157.5 (Ar*C*), 150.8 (Ar*C*), 143.3 (Ar*C*), 140.9 (Ar*C*), 138.6 (Ar*C*), 138.3 (Ar*C*), 130.3 (Ar*C*), 129.3 (Ar*C*), 127.6 (Ar*C*), 126.2 (Ar*C*), 124.1 (Ar*C*), 122.7 (Ar*C*), 122.2 (Ar*C*), 119.6 (Ar*C*), 36.0 (tbu*C*), 34.9 (tbu*C*), 32.0 (tbu*C*), 30.3 (tbu*C*). ESI-MS (m/z): [$^{tbu}dh^{Ph}phen(H)_2$] calc'd: 740.4342 found: 740.4342.

Synthesis of Cr($^{tbu}dh^{Ph}phen$)Cl(H_2O) (1)

Metalation of $^{tbu}dh^{Ph}phen(H)_2$ with Cr(III) to generate Cr($^{tbu}dh^{Ph}phen$)Cl(H_2O) (**1**) was achieved by stirring $^{tbu}dh^{Ph}phen(H)_2$ (0.190 g, 0.256 mmol) and 1.05 equivalents of chromium (II) dichloride (0.0331 g, 0.269 mmol) in tetrahydrofuran (75 mL) at room temperature under an inert atmosphere for 3 days. After exposing the reaction to air, the THF was removed under reduced pressure. Methanol was added to the flask to precipitate unreacted ligand and metal salt which was collected via filtration. The methanol was then removed under reduced pressure and the resulting red solid was dissolved in dichloromethane and extracted with brine (3 x 75 mL) and saturated ammonium chloride (5 x 100 mL). The organic layer was then dried over $MgSO_4$ and condensed under reduced pressure to leave a dark red crystalline solid. Water was added to the roundbottom and sonicated for several minutes to suspend the solid material. This solid was collected via vacuum filtration and was washed with 200 mL of hot pentanes for a 75.8% isolated yield (0.164 g). Elemental analysis for $C_{52}H_{56}ClCrN_2O_3$•0.5(CH_2Cl_2) calc'd: C 71.10, H 6.48, N 3.16; found: C 71.45, H 6.54, N 3.22. ESI-MS (m/z): [Cr($^{tbu}dh^{Ph}phen$)]–Cl–H_2O calc'd: 790.3590 found: 790.3582.

Synthesis of Cr($^{tbu}dhphen$)Cl(H_2O) (2)

The synthesis of Cr($^{tbu}dhphen$)Cl(H_2O) was carried out as previously reported.[4]

Synthesis of Cr(^{tbu}dh^{tbu}bpy)Cl(H_2O) (3)

The synthesis of Cr(^{tbu}dh^{tbu}bpy)Cl(H_2O) was carried out as previously reported.[5]

Synthesis of Benzonaphthothiophene 7,7-dioxide, BNTD

Benzonaphthothiophene (0.581 g, 2.48 mmol) was suspended in acetic acid (25 mL). While stirring at room temperature, 30% hydrogen peroxide (19 mL) was added dropwise to the mixture. The flask was then refluxed overnight and the precipitate changed from white to light yellow. After cooling the reaction to room temperature, the precipitate was collected via filtration and washed with water and diethyl ether for a 47.5% isolated yield (0.313 g). ^{1}H NMR (DMSO-d_6, 600 MHz): δ 8.96 (d, 1H, Ar*H*), 8.79 (d, 1H, Ar*H*), 8.30 (d, 1H, Ar*H*), 8.21 (d, 1H, Ar*H*), 8.09 (d, 1H, Ar*H*), 8.02 (d, 1H, Ar*H*), 7.88 (m, 2H, Ar*H*), 7.81 (t, 1H, Ar*H*), 7.73 (t, 1H, Ar*H*). ^{13}C{^{1}H} NMR (DMSO-d_6, 150 MHz): δ 137.4 (Ar*C*), 136.4 (Ar*C*), 135.3 (Ar*C*), 134.8 (Ar*C*), 132.7 (Ar*C*), 131.3 (Ar*C*), 130.4 (Ar*C*), 130.0 (Ar*C*), 129.6 (Ar*C*), 128.9 (Ar*C*), 128.0 (Ar*C*), 127.2 (Ar*C*), 126.1 (Ar*C*), 125.2 (Ar*C*), 122.4 (Ar*C*), 116.8 (Ar*C*). Elemental analysis for $C_{16}H_{10}O_2S$ calc'd: C 72.16, H 3.79, N 0.00; found: C 71.91, H 3.62, N 0.01. ESI-MS (m/z): [BNTD] calc'd: 266.0402 found: 266.0401.

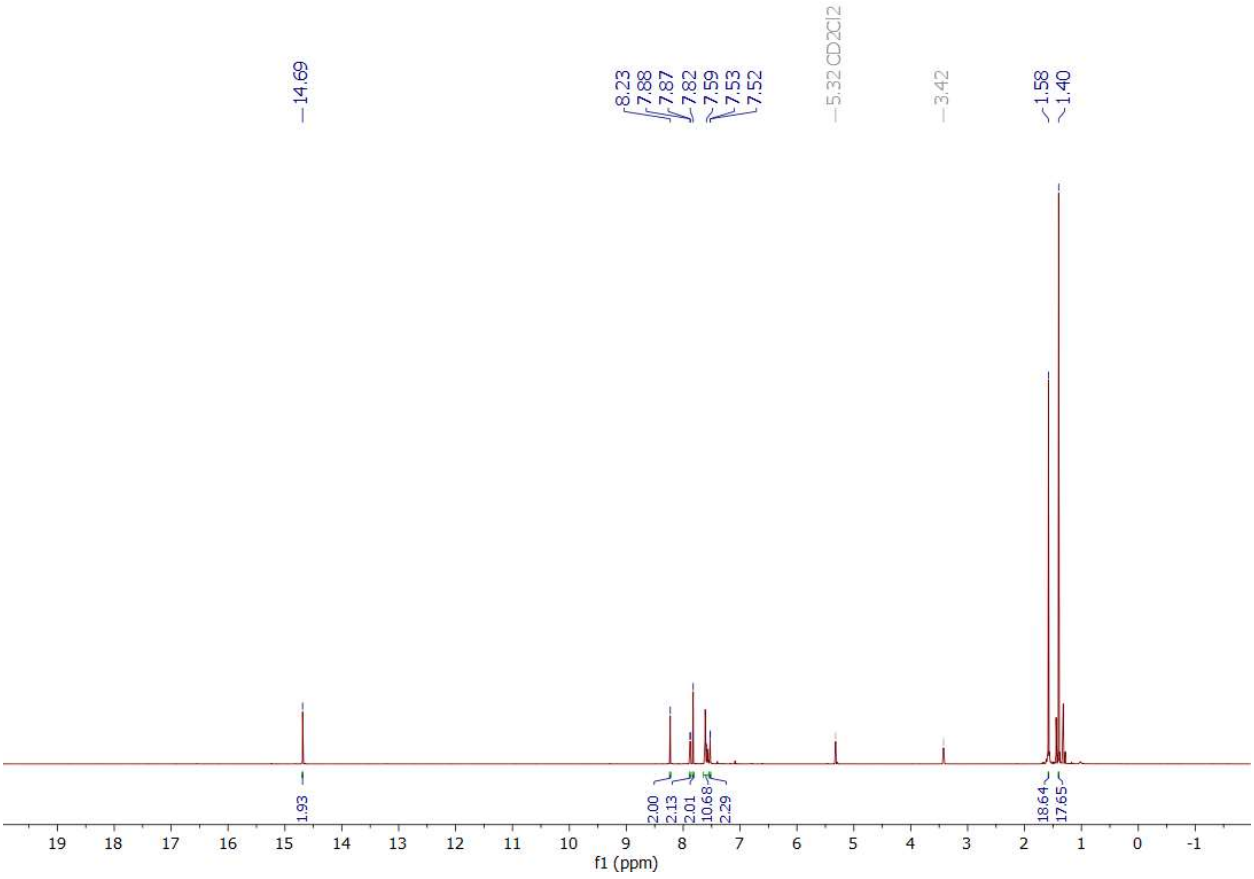

Figure S1. ^{1}H NMR of ^{tbu}dh^{Ph}phen(H)$_2$ ligand; CD_2Cl_2; 600 MHz.

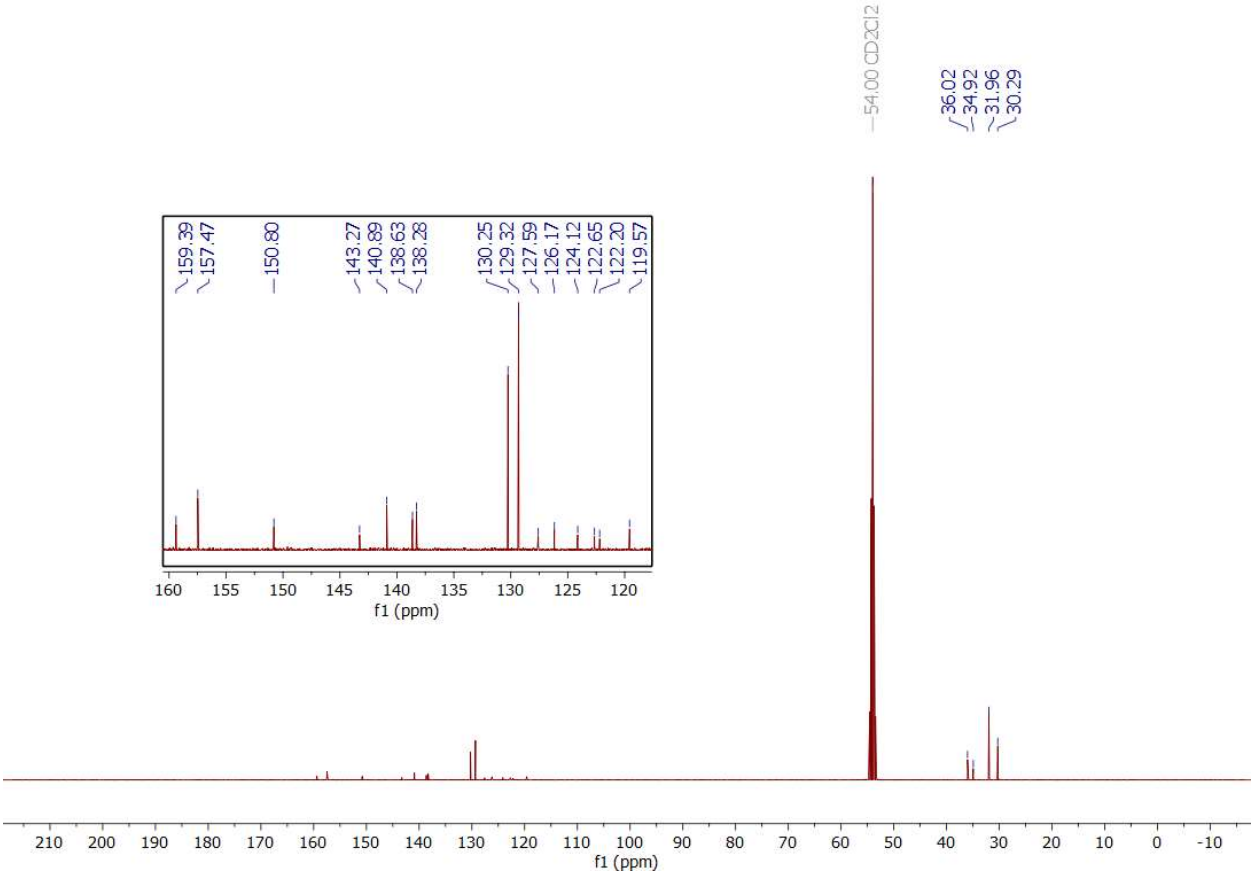

Figure S2. ^{13}C {^{1}H} NMR of $^{tbu}dh^{Ph}phen(H)_2$ ligand; CD_2Cl_2; 100 MHz.

Evans' Method Characterization of 1

The spin state of the Cr($^{tbu}dh^{Ph}phen$)Cl(H_2O) (**1**) catalyst was characterized as a Cr(III) species via Evans' Method.[18, 19] Three capillary inserts were made with a 50% v/v mixture of DMF and DMF-d_7. Each insert was flame sealed, and then placed in an NMR tube. Then 6.5 mg of **1** was dissolved in 3 mL of DMF. Approximately 0.6 mL of the solution of **1** was added to each of the three NMR tubes containing a flame sealed insert. ^{1}H NMR spectra with 64 scans were then taken using a 600 MHz Varian NMR Spectrometer. The results of this experiment, which was run in triplicate, can be seen in **Table S2**. The average μ_{eff} of 1 was 4.2±0.1.

Table S2. Evans' method results for Cr($^{tbu}dh^{Ph}phen$)Cl(H_2O) (**1**) in DMF.[18, 19]

Trial	Chemical Shift (ppm)	Chemical Shift (Hz)	Total Magnetic Moment (emu mol^{-1})	Paramagnetic Moment (emu mol^{-1})	μ_{eff} (Bohr Magnetons)
1	0.08	32.0	0.00744	7.98×10^{-3}	4.36
2	0.08	32.0	0.00744	7.98×10^{-3}	4.36
3	0.07	28.0	0.00651	7.05×10^{-3}	4.10

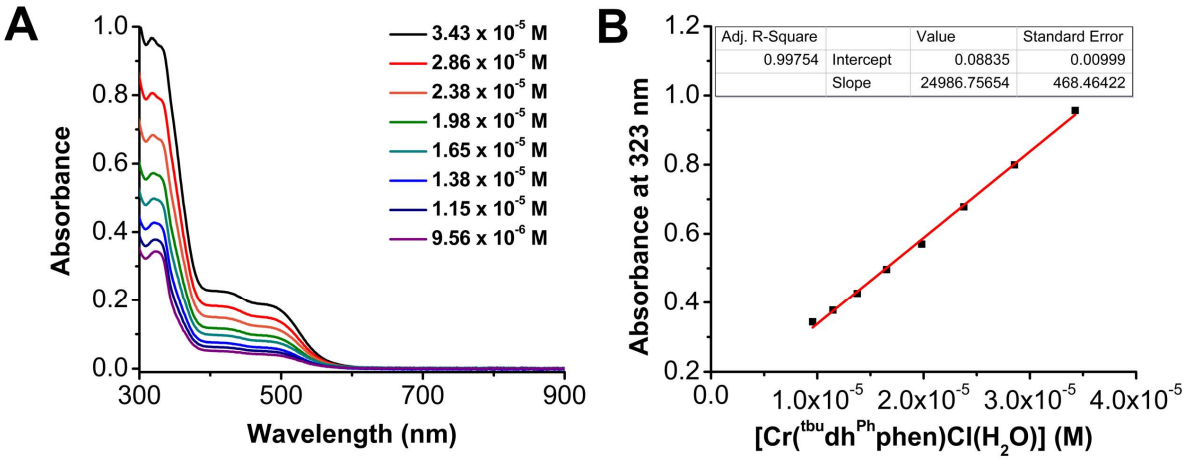

Figure S3. (**A**) UV-vis serial dilution absorbance data obtained from Cr(^{tbu}dh^{Ph}phen)Cl(H_2O) **1** in a DMF solution. Conditions: varying concentration of **1**; quartz cell with 1 cm pathlength. (**B**) Plot of absorbance versus concentration (M) for Cr(^{tbu}dh^{Ph}phen)Cl(H_2O) **1** in DMF at 323 nm (25000 M^{-1} cm^{-1}); R^2 = 0.997. All: λ_{max} = 425 nm (7040 M^{-1} cm^{-1}) and 490 nm (5860 M^{-1} cm^{-1}).

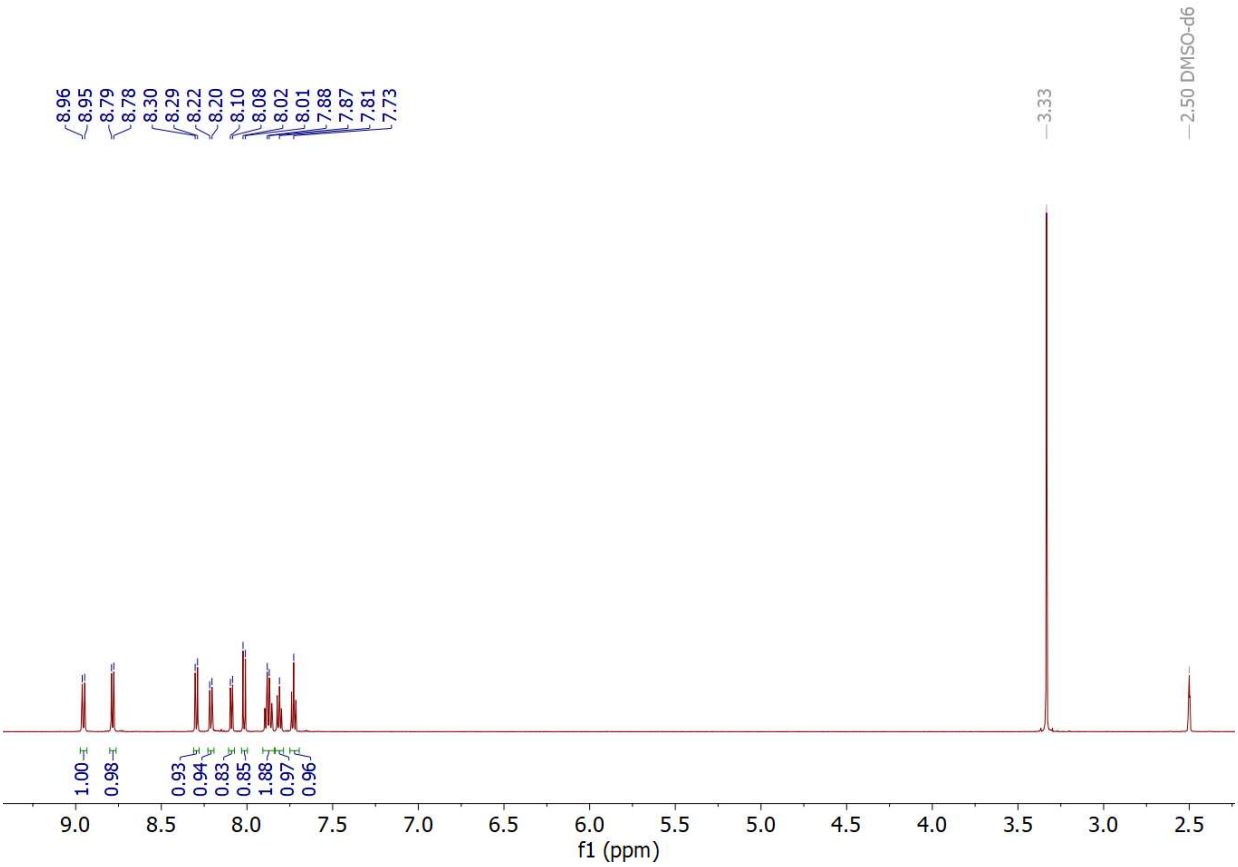

Figure S4. ^{1}H NMR of BNTD; DMSO-d_6; 600 MHz.

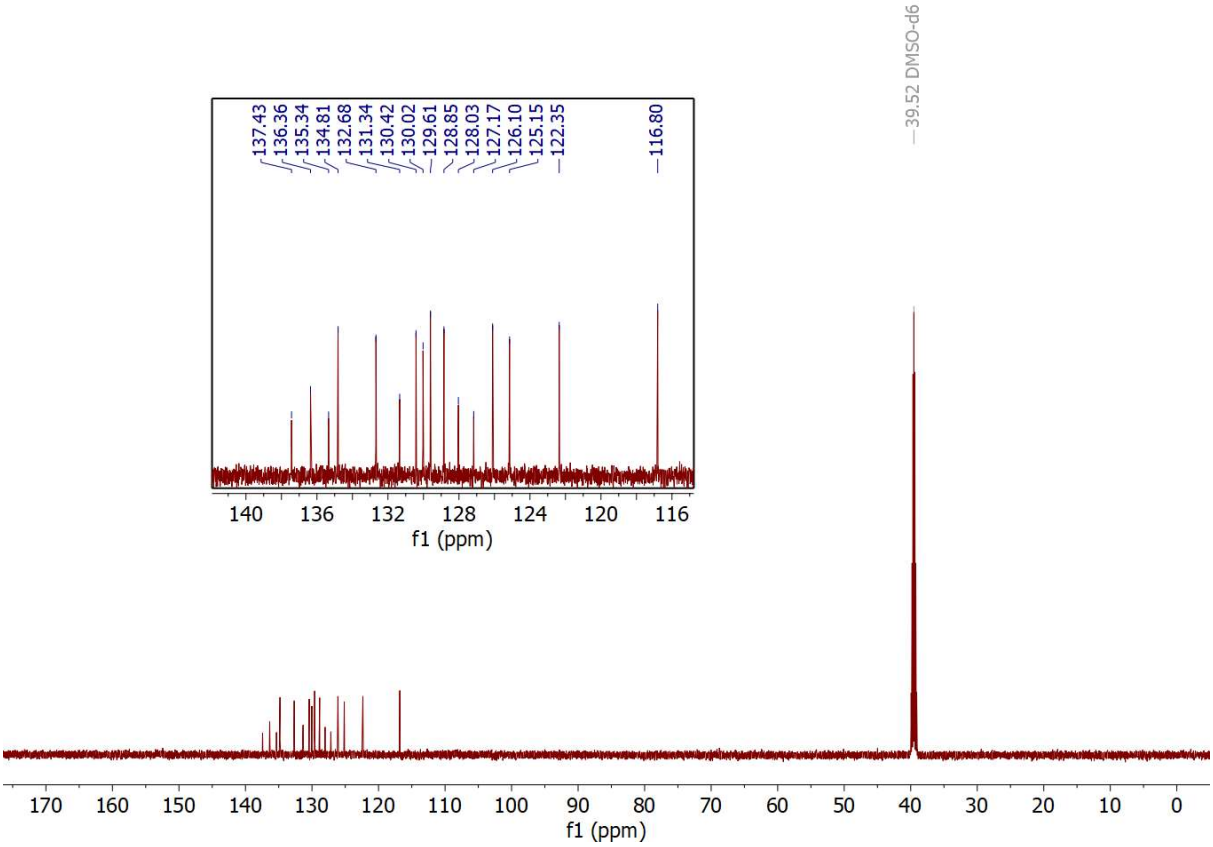

Figure S5. ^{13}C {^{1}H} NMR of BNTD; DMSO-d_6; 150 MHz.

Electrochemistry of 1

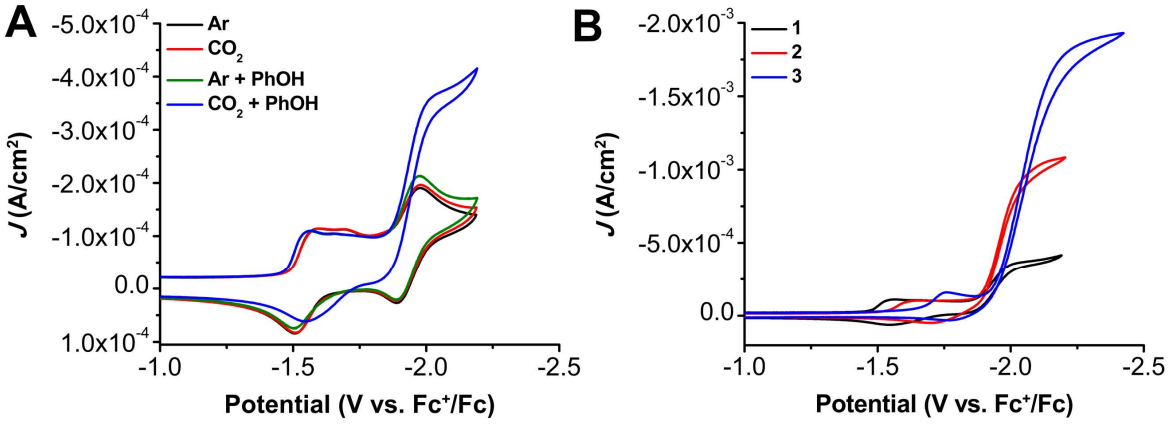

Figure S6. (**A**) CVs of 1.0 mM Cr(^{tbu}dh^{Ph}phen)Cl(H_2O) **1** with and without 0.5 M PhOH under Ar and CO_2 saturation conditions.(**B**) CVs of Cr(^{tbu}dh^{Ph}phen)Cl(H_2O) **1**, Cr(^{tbu}dhphen)Cl(H_2O) **2**, and Cr(^{tbu}dh^{tbu}bpy)Cl(H_2O) **3** with 0.5 M PhOH under CO_2 saturation conditions.Conditions: 0.1 M $TBAPF_6$/DMF; glassy carbon disc working electrode, glassy carbon rod counter electrode, Ag/AgCl pseudoreference electrode; referenced to Fc^+/Fc internal standard; 100 mV/s scan rate.

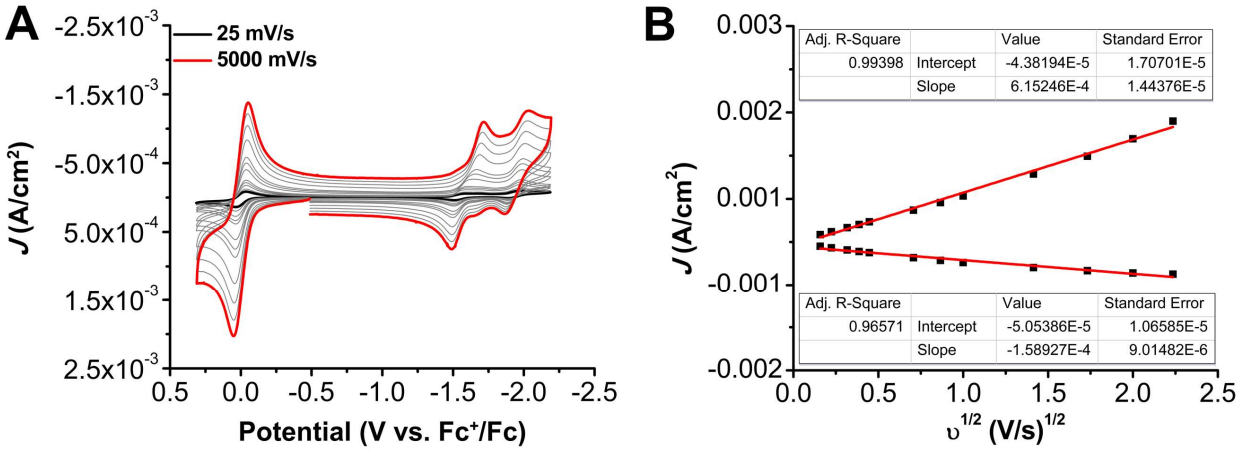

Figure S7. (**A**) CVs of Cr(^{tbu}dh^{Ph}phen)Cl(H_2O) **1** at variable scan rates ranging from 25 (black) to 5000 (red) mV/s, obtained under Ar saturation conditions. (**B**) Linear Fit of variable scan rate data from (**A**) demonstrating that Cr(^{tbu}dh^{Ph}phen)Cl(H_2O) **1** shows a diffusion-limited current response. The data in (**B**) was obtained from the reversible redox feature at −1.93 V vs Fc^+/Fc. Conditions: 1.0 mM **1**, 0.1 M $TBAPF_6$/DMF; glassy carbon working electrode, glassy carbon counter electrode, Ag/AgCl pseudoreference electrode; varied scan rate; referenced to internal ferrocene standard.

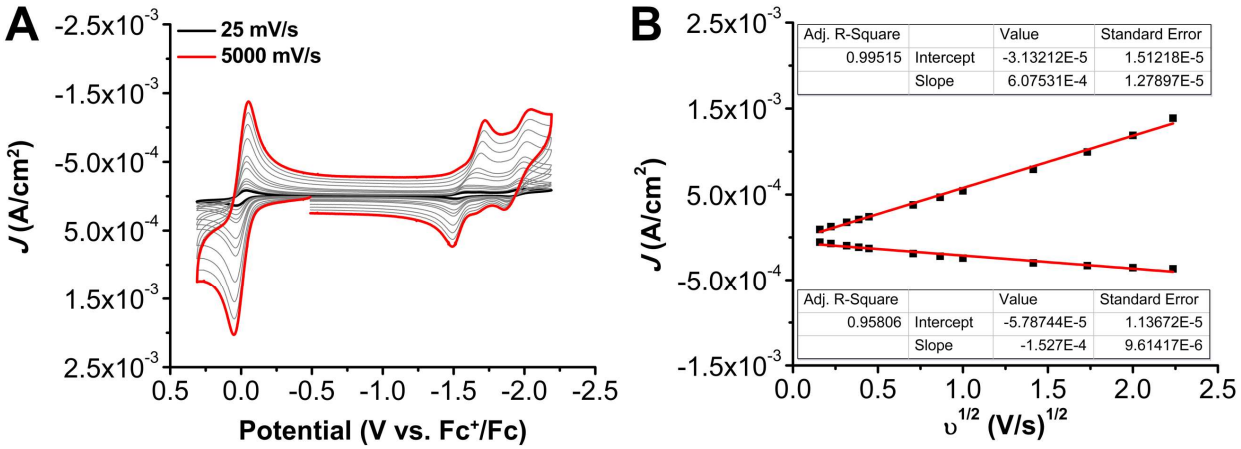

Figure S8. (**A**) CVs of Cr(^{tbu}dh^{Ph}phen)Cl(H_2O) **1** at variable scan rates ranging from 25 (black) to 5000 (red) mV/s, obtained under CO_2 saturation conditions. (**B**) Linear Fit of variable scan rate data from (**A**) demonstrating that Cr(^{tbu}dh^{Ph}phen)Cl(H_2O) **1** shows a diffusion-limited current response. The data in (**B**) was obtained from the reversible redox feature at −1.93 V vs Fc^+/Fc. Conditions: 1.0 mM 1, 0.1 M $TBAPF_6$/DMF; glassy carbon working electrode, glassy carbon counter electrode, Ag/AgCl pseudoreference electrode; varied scan rate; referenced to internal ferrocene standard.

At high scan rates in **Figures S7** and **S8**, the first two reduction features condense into a single feature, consistent with outcompeting a solvent-displacement equilibrium as summarized below, where L = ^{tbu}dh^{Ph}phen^{2-} and S = solvent and E_1^0 and E_2^0 are the first and second reduction features observed at 100 mV/s.

$$[Cr(L)Cl] + e^- \rightleftharpoons [Cr(L)Cl]^- \qquad E_1^0$$

$$[Cr(L)Cl]^0 + S \rightleftharpoons [Cr(L)(S)]^+ + Cl^-$$

$$[Cr(L)(S)]^+ + e^- \rightleftharpoons [Cr(L)(S)]^0 \qquad E_2^0$$

For all variable concentration studies without the presence of RMs (**Figures S9-S11**) analysis was adapted from Sathrum and Kubiak J. Phys. Chem. Lett. **2011**, *2*, 2372.[20] *F* is Faraday's constant, *A* is the electrode area, [*Q*] is the substrate concentration, k_{cat} is the catalytic rate, *D* is the diffusion constant of the catalyst, [*cat*] is the concentration of the catalyst, and n_{cat} is the number of electrons involved in the catalytic process.

$$\boldsymbol{i_{cat} = n_{cat}FA[cat](Dk_{cat}[Q]^y)^{1/2}}$$

*For all concentration experiments in **Figure S9-S11**, only points where fully irreversible catalytic features are observed outside of the saturation range were included in the linear fits.*

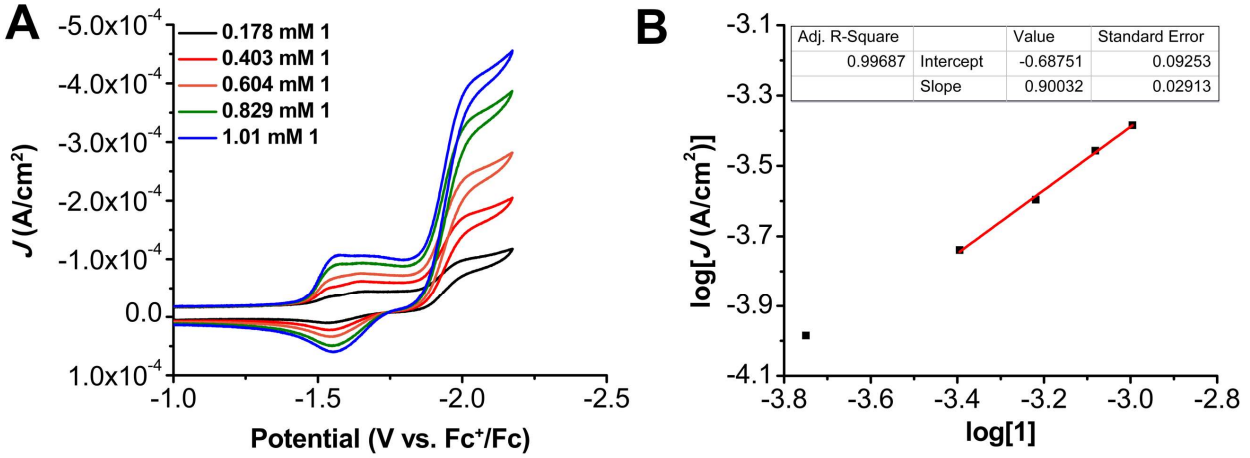

Figure S9. (**A**) CVs of Cr(^{tbu}dh^{Ph}phen)Cl(H_2O) **1** at variable concentrations, obtained under CO_2 saturation with 0.6 M PhOH. Conditions: 0.1 M $TBAPF_6$/DMF; glassy carbon disc working electrode, glassy carbon rod counter electrode, Ag/AgCl pseudoreference electrode; 100 mV/s scan rate; referenced to internal ferrocene standard. (**B**) Log-log plot from data obtained from CVs in **A** at −2.06 V vs. Fc^+/Fc.

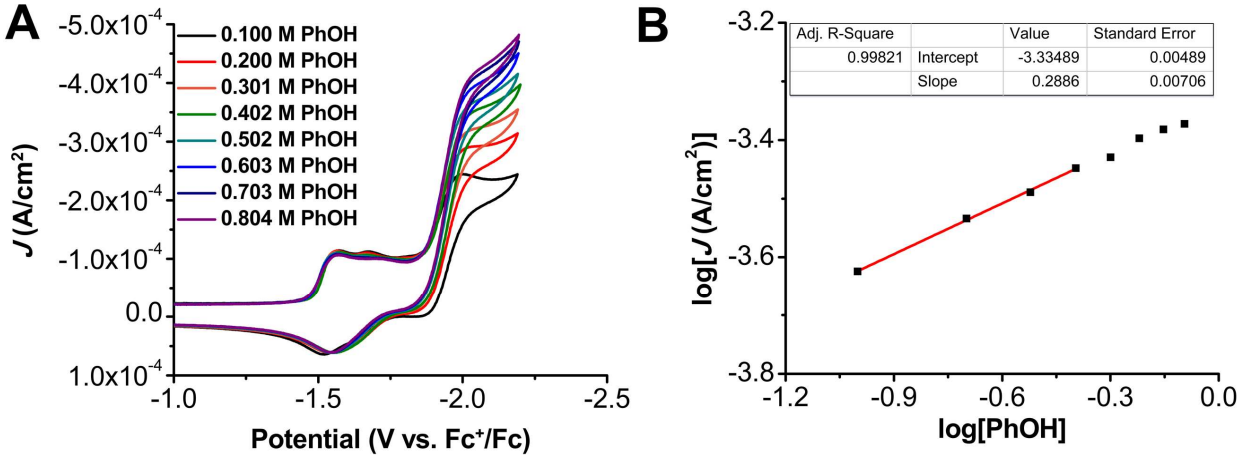

Figure S10. (**A**) CVs of 1.0 mM Cr(^{tbu}dh^{Ph}phen)Cl(H_2O) **1**, obtained under CO_2 saturation conditions with variable PhOH concentrations. Conditions: 0.1 M $TBAPF_6$/DMF; glassy carbon disc working electrode, glassy carbon rod counter electrode, Ag/AgCl pseudoreference electrode; 100 mV/s scan rate; referenced to internal ferrocene standard. (**B**) Log-log plot from data obtained from CVs in **A** at −2.06 V vs. Fc^+/Fc.

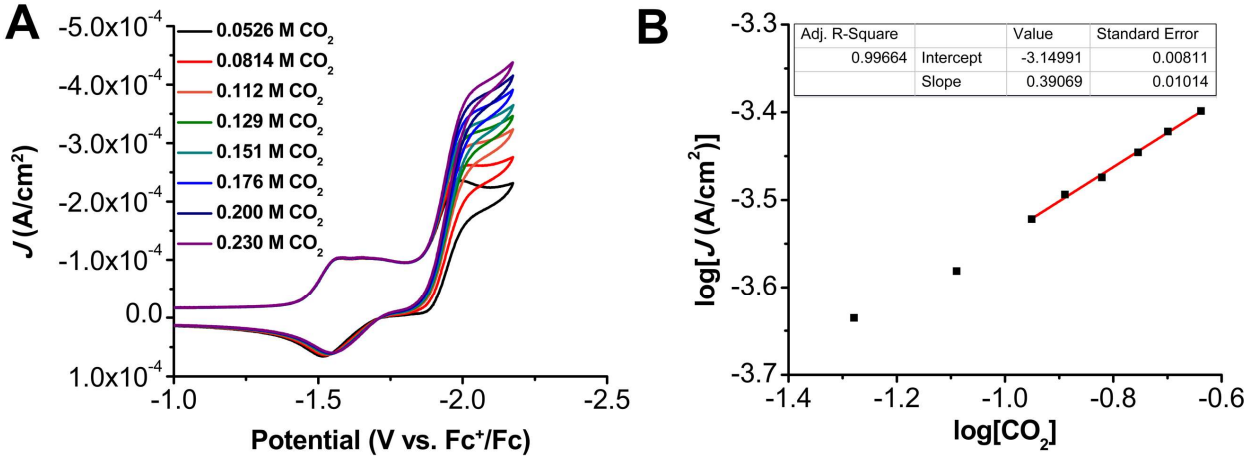

Figure S11. (**A**) CVs of 1.0 mM Cr(^{tbu}dh^{Ph}phen) **1** obtained under variable CO_2 concentrations with 0.6 M PhOH. Conditions: 0.1 M $TBAPF_6$/DMF; glassy carbon disc working electrode, glassy carbon rod counter electrode, Ag/AgCl pseudoreference electrode; 100 mV/s scan rate; referenced to internal ferrocene standard. (**B**) Log-log plot from data obtained from CVs in **A** at −2.06 V vs. Fc^+/Fc.

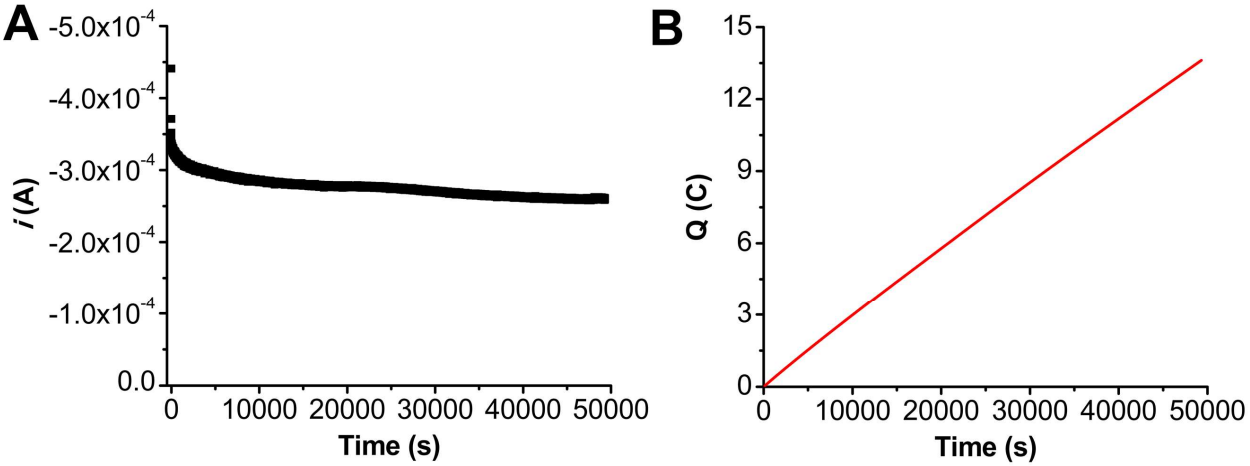

Figure S12. (**A**) Current versus time trace from CPE experiment for **1**+PhOH. (**B**) Charge passed versus time for the CPE experiment shown in **A**. Conditions were 0.5 mM Cr(^{tbu}dh^{Ph}phen)Cl(H_2O) **1** and 0.8 M PhOH under a CO_2 atmosphere at −2.10 V vs Fc^+/Fc in 0.1 M $TBAPF_6$/DMF; working electrode was a glassy carbon rod, counter electrode was a graphite rod, and the reference was a nonaqueous Ag/AgCl pseudoreference electrode; 0.075 M Fc was used as sacrificial oxidant.

Table S3. Results from CPE experiment in **Figure S12**, **1** + 0.8 M PhOH.

Time (s)	Charge (coulombs)	Moles (e^-)	Moles of CO	FE_{CO}	Moles of H_2	FE_{H2}
49329*	13.6	1.41×10^{-4}	6.58×10^{-5}	93.3	2.95×10^{-6}	4.18
49329*	13.6	1.41×10^{-4}	6.51×10^{-5}	92.2	4.67×10^{-6}	6.61
49329*	13.6	1.41×10^{-4}	6.40×10^{-5}	90.7	3.85×10^{-6}	5.45
49329*	13.6	1.41×10^{-4}	6.41×10^{-5}	90.9	2.17×10^{-6}	3.07
49329*	13.6	1.41×10^{-4}	6.06×10^{-5}	85.8	6.20×10^{-6}	8.79

*indicates a series of injections carried out upon completion of electrolysis

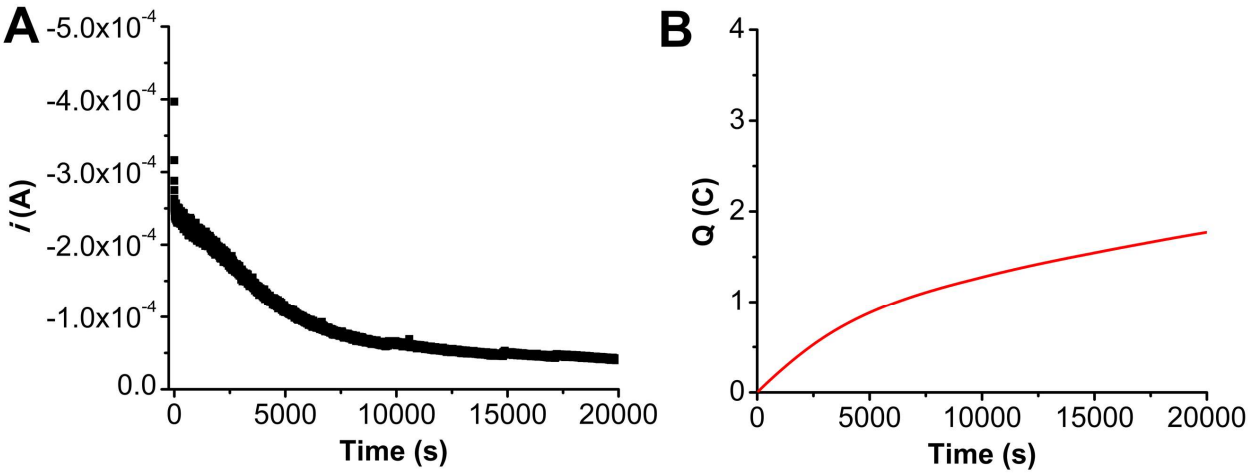

Figure S13. (**A**) Current versus time trace from CPE experiment for **1**. (**B**) Charge passed versus time for the CPE experiment shown in **A**. Conditions were 0.5 mM Cr(^{tbu}dh^{Ph}phen)Cl(H_2O) **1** under a CO_2 atmosphere at −2.10 V vs Fc^+/Fc in 0.1 M $TBAPF_6$/DMF; working electrode was a glassy carbon rod, counter electrode was a graphite rod, and the reference was a nonaqueous Ag/AgCl pseudoreference electrode; 0.075 M Fc was used as sacrificial oxidant.

Table S4. Results from CPE experiment in **Figure S13**, **1**.

Time (s)	Charge (coulombs)	Moles (e^-)	Moles of CO
9633	1.25	1.30×10^{-5}	< LOQ
14803	1.54	1.59×10^{-5}	< LOQ
17157	1.65	1.71×10^{-5}	< LOQ
19999	1.77	1.84×10^{-5}	< LOQ

Electrochemistry of BNTD

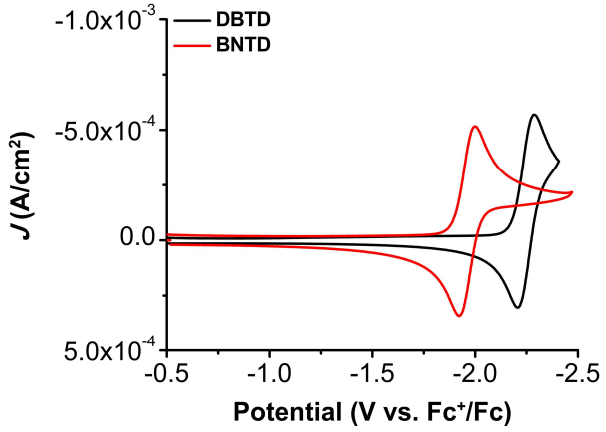

Figure S14. CVs of 2.5 mM DBTD and BNTD obtained under Ar saturation conditions. Conditions: 0.1 M $TBAPF_6$/DMF; glassy carbon disc working electrode, glassy carbon rod counter electrode, Ag/AgCl pseudoreference electrode; referenced to Fc^+/Fc internal standard; 100 mV/s scan rate.

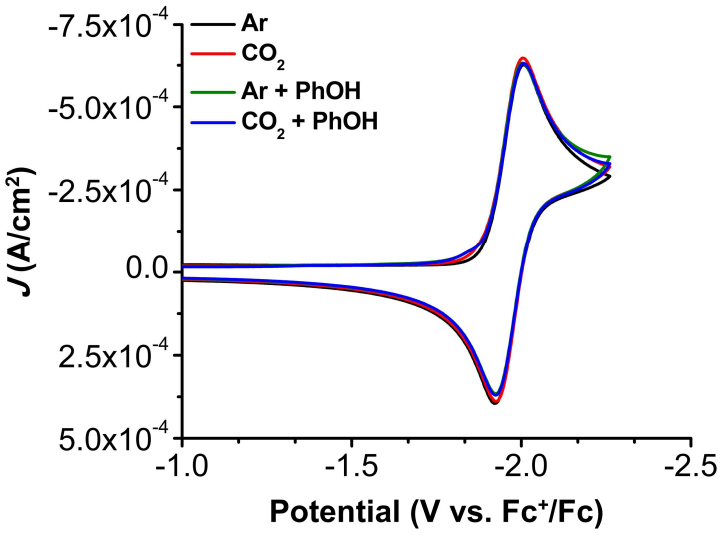

Figure S15. CVs of 2.5 mM BNTD both with and without 0.1 M PhOH obtained under Ar and CO_2 saturation conditions. Conditions: 0.1 M $TBAPF_6$/DMF; glassy carbon disc working electrode, glassy carbon rod counter electrode, Ag/AgCl pseudoreference electrode; referenced to Fc^+/Fc internal standard; 100 mV/s scan rate.

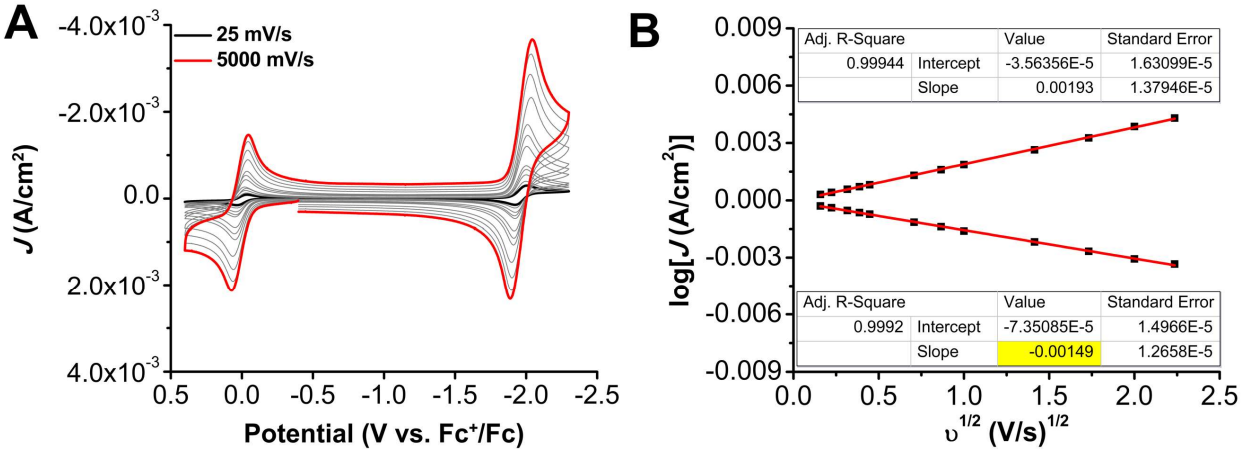

Figure S16. (**A**) CVs of 2.5 mM BNTD at variable scan rates ranging from 25 (black) to 5000 (red) mV/s, obtained under Ar saturation conditions. (**B**) Linear Fit of variable scan rate data from **A** demonstrating that BNTD shows a diffusion-limited current response. The slope highlighted in yellow was used to calculate the diffusion coefficient. The data in **B** was obtained from the reversible redox feature at −1.93 V vs Fc^+/Fc. Conditions: 0.1 M $TBAPF_6$/DMF; glassy carbon disc working electrode, glassy carbon rod counter electrode, Ag/AgCl pseudoreference electrode; varied scan rate; referenced to internal ferrocene standard.

Cyclic Voltammetry with Cr catalysts and RMs

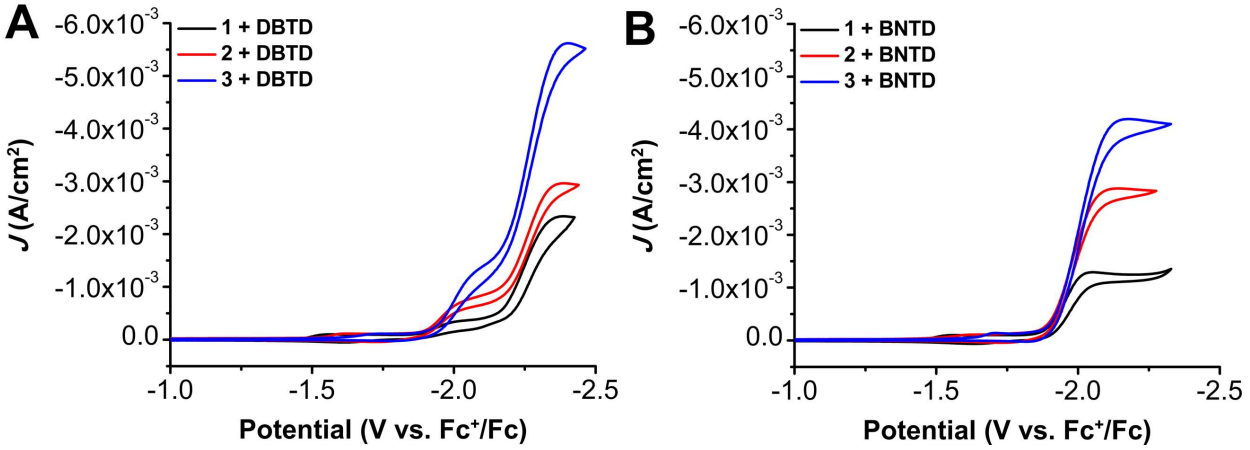

Figure S17. Comparison CVs of 1.0 mM Cr(^{tbu}dh^{Ph}phen)Cl(H_2O) **1**, Cr(^{tbu}dhphen)Cl(H_2O) **2**, and Cr(^{tbu}dh^{tbu}bpy)Cl(H_2O) **3** with (**A**) 2.5 mM DBTD and (**B**) BNTD and 0.5 M PhOH under CO_2 saturation conditions.Conditions: 0.1 M $TBAPF_6$/DMF; glassy carbon disc working electrode, glassy carbon rod counter electrode, Ag/AgCl pseudoreference electrode; referenced to Fc^+/Fc internal standard; 100 mV/s scan rate.

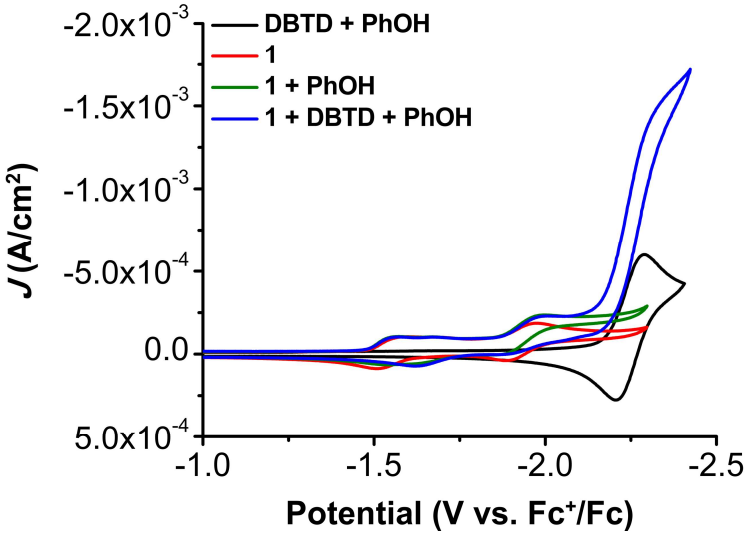

Figure S18. Comparison CVs of 1.0 mM Cr(^{tbu}dh^{Ph}phen)Cl(H_2O) **1** with and without 2.5 mM DBTD and 0.1 M PhOH under CO_2 saturation conditions.Conditions: 0.1 M $TBAPF_6$/DMF; glassy carbon disc working electrode, glassy carbon rod counter electrode, Ag/AgCl pseudoreference electrode; referenced to Fc^+/Fc internal standard; 100 mV/s scan rate.

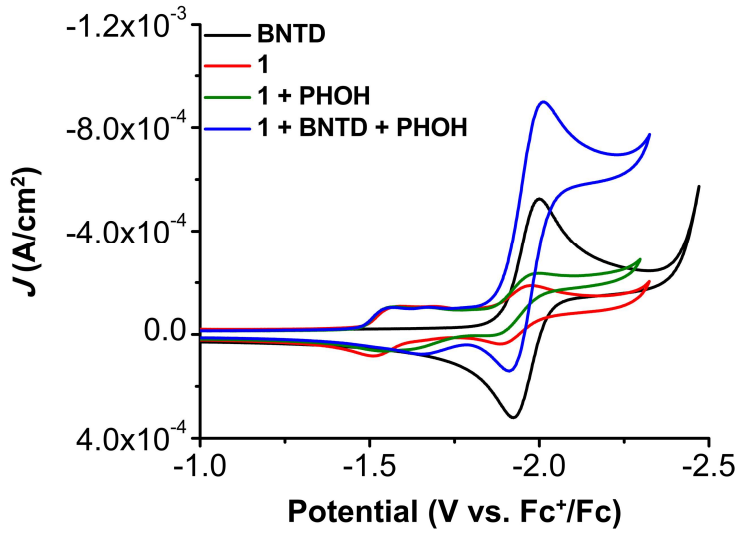

Figure S19. Comparison CVs of 1.0 mM Cr(^{tbu}dh^{Ph}phen)Cl(H_2O) **1** with and without 2.5 mM BNTD and 0.1 M PhOH under CO_2 saturation conditions.Conditions: 0.1 M $TBAPF_6$/DMF; glassy carbon disc working electrode, glassy carbon rod counter electrode, Ag/AgCl pseudoreference electrode; referenced to Fc^+/Fc internal standard; 100 mV/s scan rate.

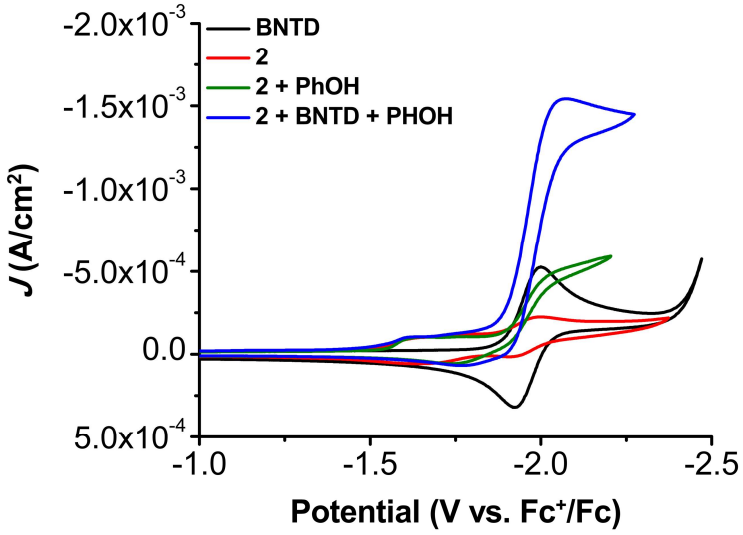

Figure S20. Comparison CVs of 1.0 mM Cr(^{tbu}dhphen)Cl(H_2O) **2** with and without 2.5 mM BNTD and 0.1 M PhOH under CO_2 saturation conditions.Conditions: 0.1 M $TBAPF_6$/DMF; glassy carbon disc working electrode, glassy carbon rod counter electrode, Ag/AgCl pseudoreference electrode; referenced to Fc^+/Fc internal standard; 100 mV/s scan rate.

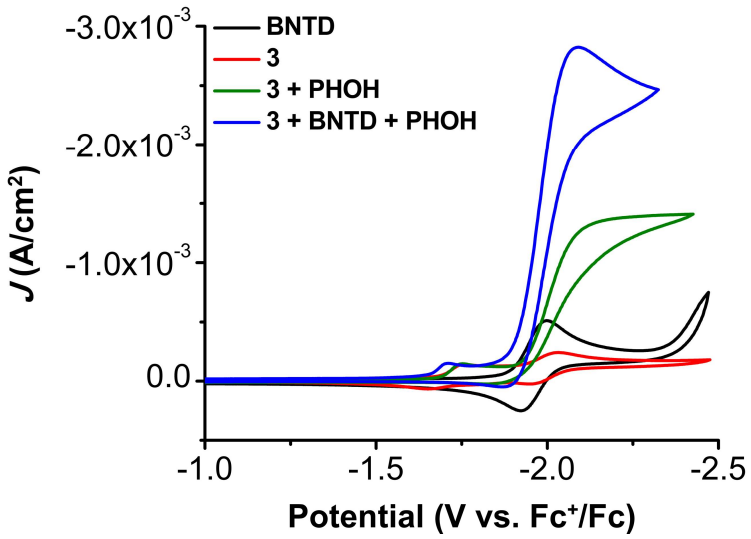

Figure S21. Comparison CVs of 1.0 mM Cr(^{tbu}dh^{tbu}bpy)Cl(H_2O) **3** with and without 2.5 mM BNTD and 0.1 M PhOH under CO_2 saturation conditions.Conditions: 0.1 M $TBAPF_6$/DMF; glassy carbon disc working electrode, glassy carbon rod counter electrode, Ag/AgCl pseudoreference electrode; referenced to Fc^+/Fc internal standard; 100 mV/s scan rate.

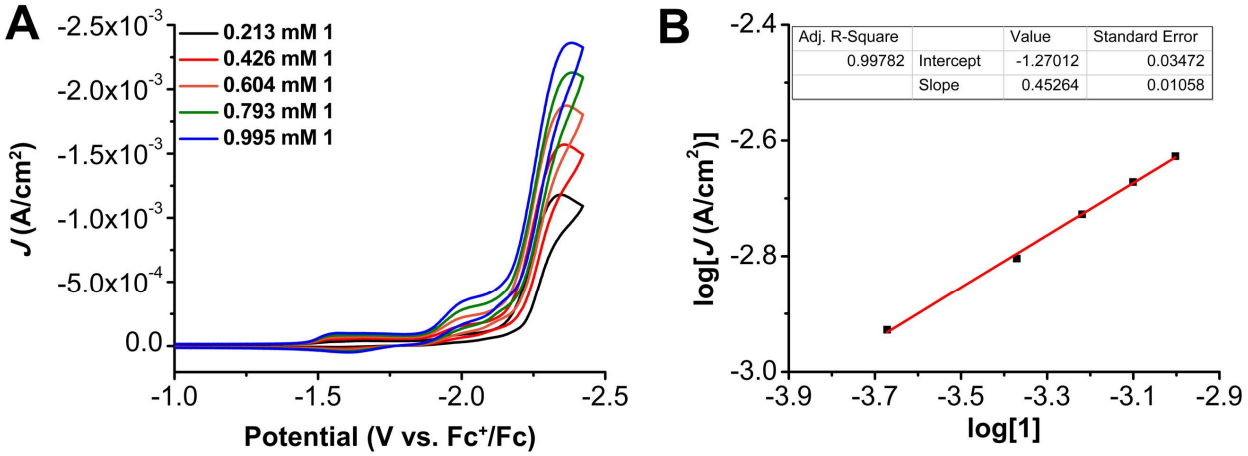

Figure S22. (**A**) CVs of Cr(^{tbu}dh^{Ph}phen)Cl(H_2O) **1** at variable concentrations, obtained under CO_2 saturation with 2.5 mM DBTD and 0.6 M PhOH. Conditions: 0.1 M $TBAPF_6$/DMF; glassy carbon disc working electrode, glassy carbon rod counter electrode, Ag/AgCl pseudoreference electrode; referenced to Fc^+/Fc internal standard; 100 mV/s scan rate. (**B**) Log-log plot from data obtained in **A** at –2.38 V vs. Fc^+/Fc.

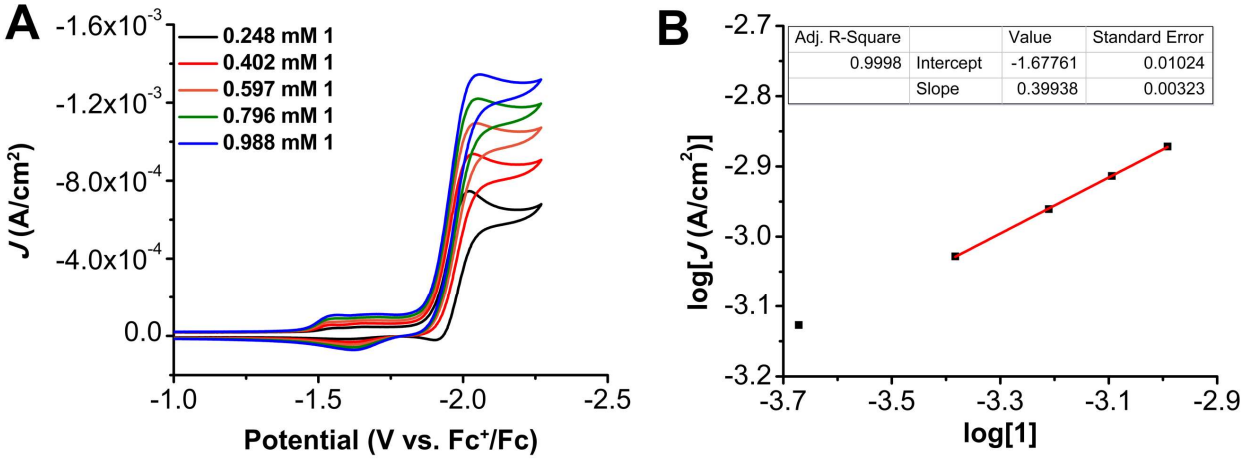

Figure S23. (**A**) CVs of Cr(^{tbu}dh^{Ph}phen)Cl(H_2O) **1** at variable concentrations, obtained under CO_2 saturation with 2.5 mM BNTD and 0.6 M PhOH. Conditions: 0.1 M $TBAPF_6$/DMF; glassy carbon disc working electrode, glassy carbon rod counter electrode, Ag/AgCl pseudoreference electrode; referenced to Fc^+/Fc internal standard; 100 mV/s scan rate. (**B**) Log-log plot from data obtained in **A** at –2.05 V vs. Fc^+/Fc.

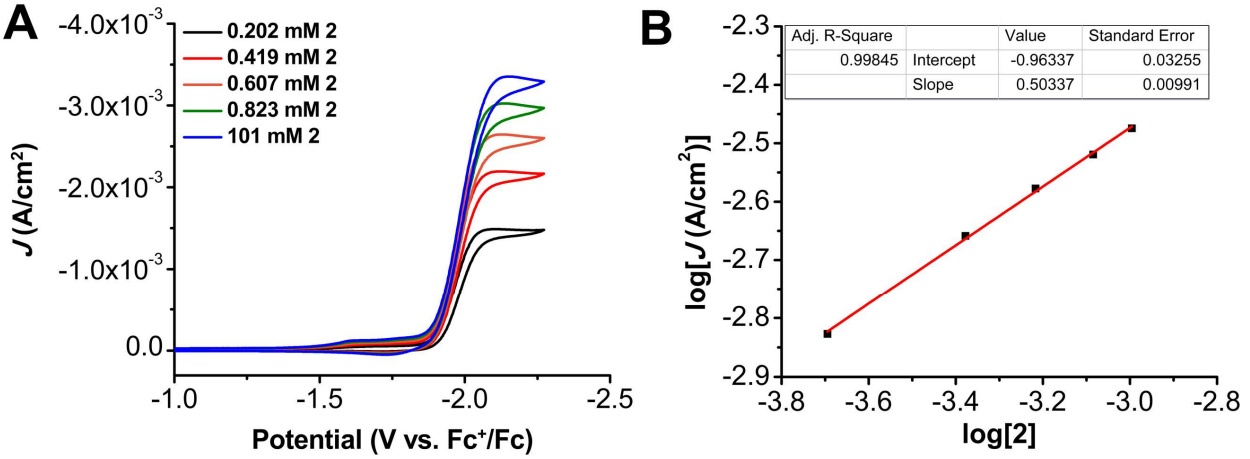

Figure S24. (**A**) CVs of Cr(^{tbu}dhphen)Cl(H_2O) **2** at variable concentrations, obtained under CO_2 saturation with 2.5 mM BNTD and 0.6 M PhOH. Conditions: 0.1 M $TBAPF_6$/DMF; glassy carbon disc working electrode, glassy carbon rod counter electrode, Ag/AgCl pseudoreference electrode; referenced to Fc^+/Fc internal standard; 100 mV/s scan rate. (**B**) Log-log plot from data obtained in **A** at –2.14 V vs. Fc^+/Fc.

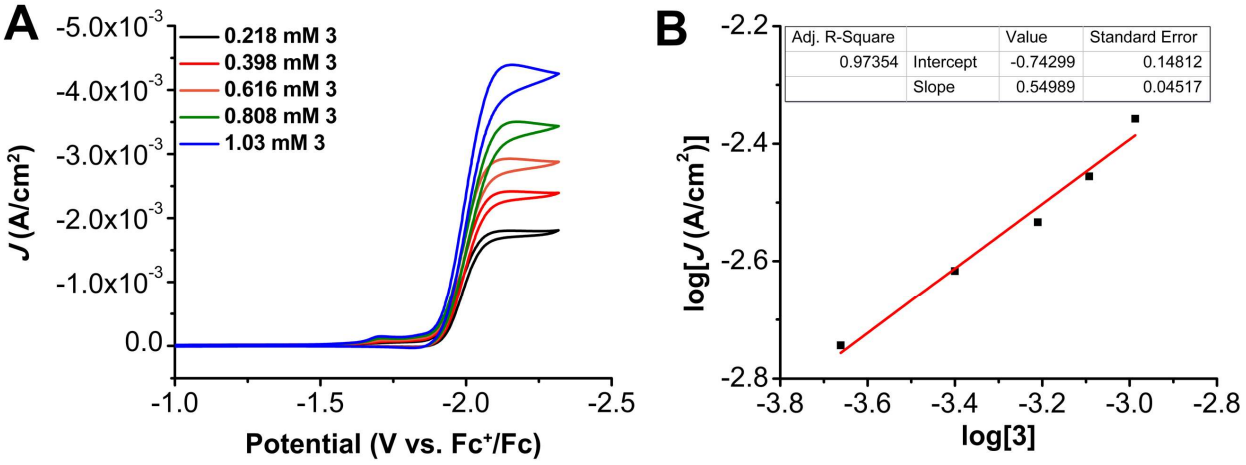

Figure S25. (**A**) CVs of Cr(^{tbu}dh^{tbu}bpy)Cl(H_2O) **3** at variable concentrations, obtained under CO_2 saturation with 2.5 mM BNTD and 0.5 M PhOH. Conditions: 0.1 M $TBAPF_6$/DMF; glassy carbon disc working electrode, glassy carbon rod counter electrode, Ag/AgCl pseudoreference electrode; referenced to Fc^+/Fc internal standard; 100 mV/s scan rate. (**B**) Log-log plot from data obtained in **A** at –2.15 V vs. Fc^+/Fc.

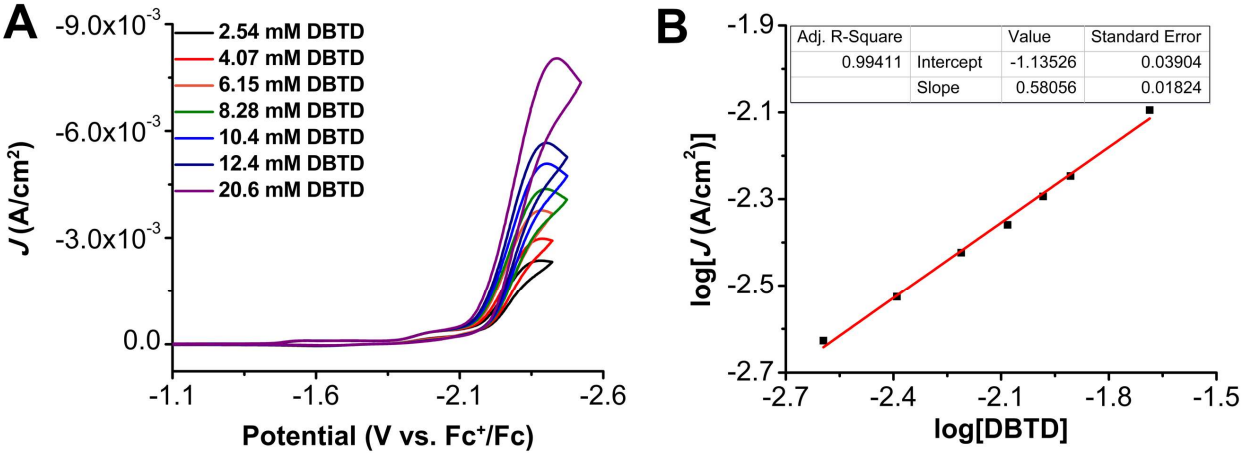

Figure S26. (**A**) CVs of 1.0 mM Cr(^{tbu}dh^{Ph}phen)Cl(H_2O) **1** with 0.6 M PhOH at variable DBTD concentrations, obtained under CO_2 saturation. Conditions: 0.1 M $TBAPF_6$/DMF; glassy carbon disc working electrode, glassy carbon rod counter electrode, Ag/AgCl pseudoreference electrode; referenced to Fc^+/Fc internal standard; 100 mV/s scan rate. (**B**) Log-log plot from data obtained in **A** at –2.37 V vs. Fc^+/Fc.

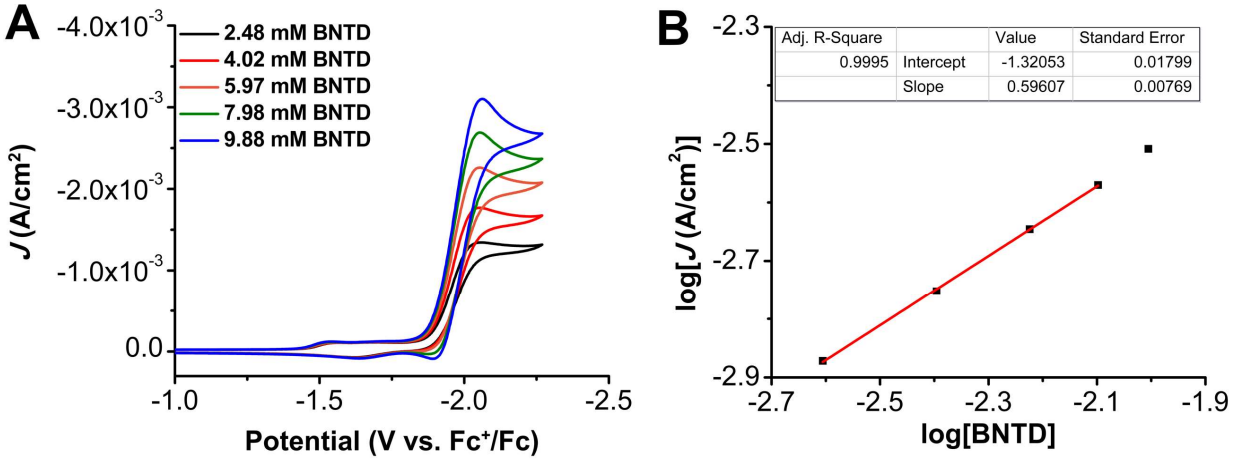

Figure S27. (**A**) CVs of 1.0 mM Cr(^{tbu}dh^{Ph}phen)Cl(H_2O) **1** with 0.6 M PhOH at variable BNTD concentrations, obtained under CO_2 saturation. Conditions: 0.1 M $TBAPF_6$/DMF; glassy carbon disc working electrode, glassy carbon rod counter electrode, Ag/AgCl pseudoreference electrode; referenced to Fc^+/Fc internal standard; 100 mV/s scan rate. (**B**) Log-log plot from data obtained in **A** at –2.06 V vs. Fc^+/Fc.

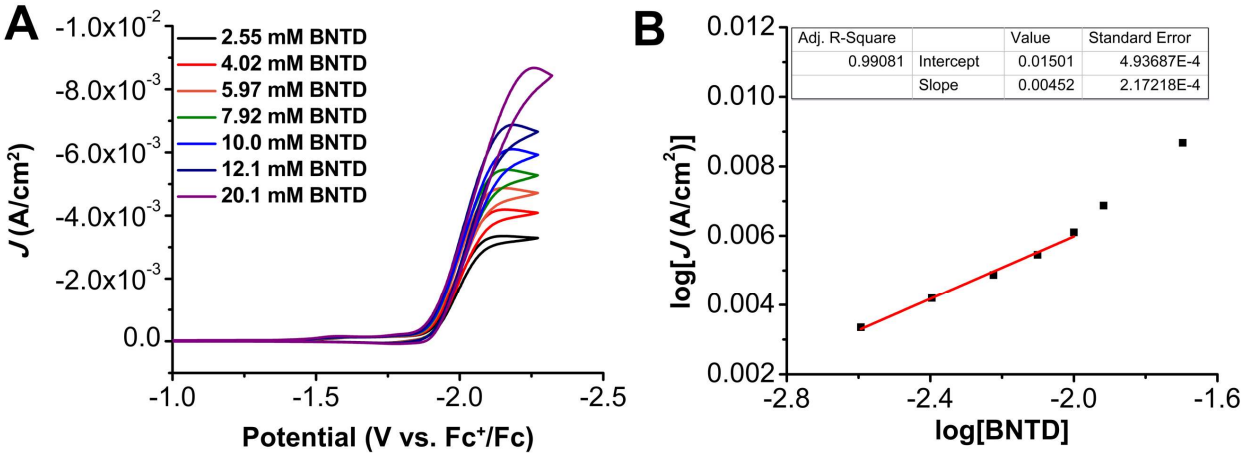

Figure S28. (**A**) CVs of 1.0 mM Cr(^{tbu}dhphen)Cl(H_2O) **2** with 0.6 M PhOH at variable BNTD concentrations, obtained under CO_2 saturation. Conditions: 0.1 M $TBAPF_6$/DMF; glassy carbon disc working electrode, glassy carbon rod counter electrode, Ag/AgCl pseudoreference electrode; referenced to Fc^+/Fc internal standard; 100 mV/s scan rate. (**B**) Log-log plot from data obtained in **A** at –2.16 V vs. Fc^+/Fc.

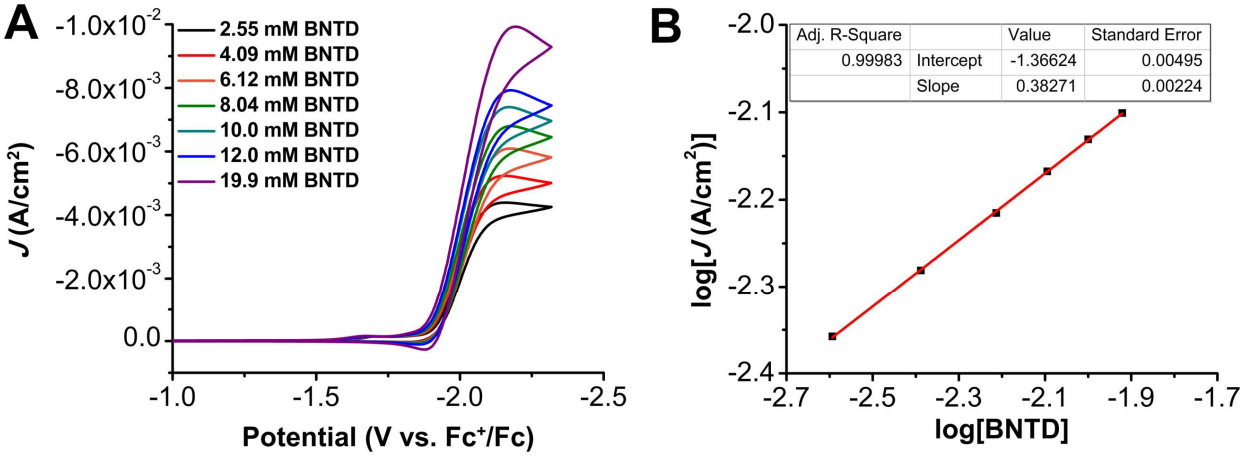

Figure S29. (**A**) CVs of 1.0 mM Cr(^{tbu}dh^{tbu}bpy)Cl(H_2O) **3** with 0.5 M PhOH at variable BNTD concentrations, obtained under CO_2 saturation. Conditions: 0.1 M $TBAPF_6$/DMF; glassy carbon disc working electrode, glassy carbon rod counter electrode, Ag/AgCl pseudoreference electrode; referenced to Fc^+/Fc internal standard; 100 mV/s scan rate. (**B**) Log-log plot from data obtained in **A** at –2.17 V vs. Fc^+/Fc.

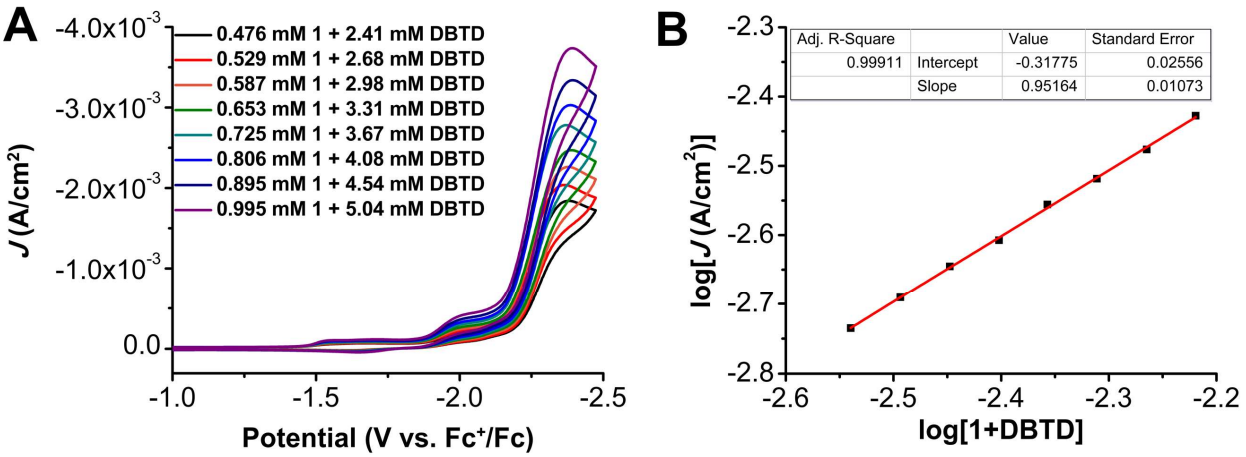

Figure S30. (**A**) CVs where the concentrations of Cr(^{tbu}dh^{Ph}phen)Cl(H_2O) **1** and DBTD were varied at a fixed 1:5 ratio of **1**:DBTD with 0.6 M PhOH under CO_2 saturation conditions. Conditions: 0.1 M $TBAPF_6$/DMF; glassy carbon disc working electrode, glassy carbon rod counter electrode, Ag/AgCl pseudoreference electrode; referenced to Fc^+/Fc internal standard; 100 mV/s scan rate. (**B**) Log-log plot from data obtained in **A** at –2.39 V vs. Fc^+/Fc.

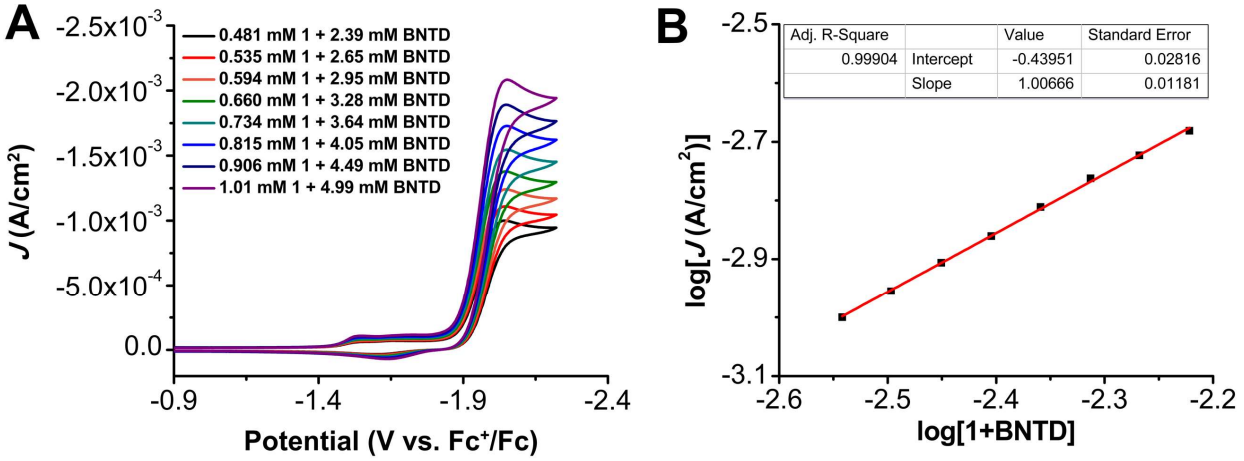

Figure S31. (**A**) CVs where the concentrations of Cr(^{tbu}dh^{Ph}phen)Cl(H_2O) **1** and BNTD were varied at a fixed 1:5 ratio of **1**:BNTD with 0.6 M PhOH under CO_2 saturation conditions. Conditions: 0.1 M $TBAPF_6$/DMF; glassy carbon disc working electrode, glassy carbon rod counter electrode, Ag/AgCl pseudoreference electrode; referenced to Fc^+/Fc internal standard; 100 mV/s scan rate. (**B**) Log-log plot from data obtained in **A** at –2.05 V vs. Fc^+/Fc.

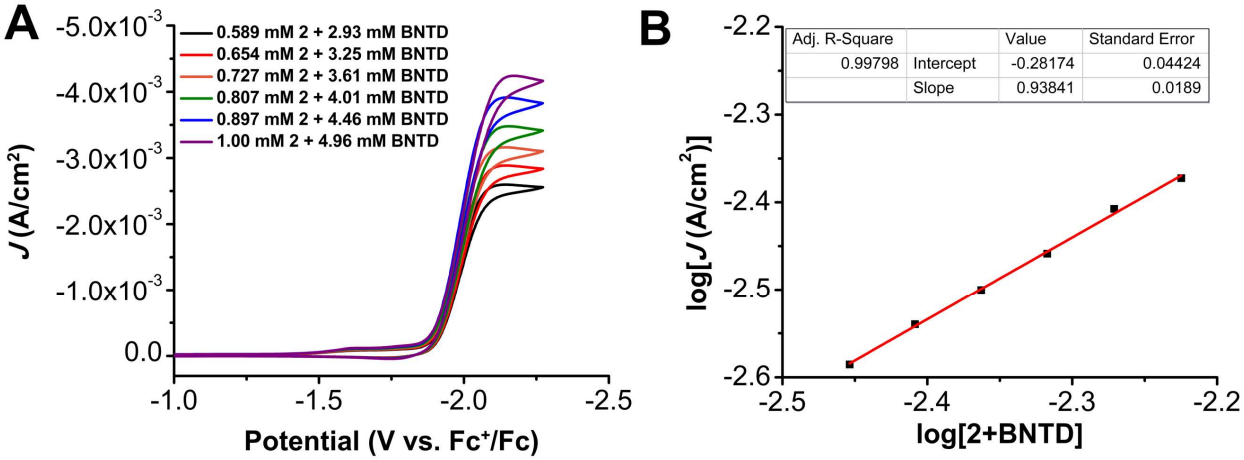

Figure S32. (**A**) CVs where the concentrations of Cr(^{tbu}dhphen)Cl(H_2O) **2** and BNTD were varied at a fixed 1:5 ratio of **2**:BNTD with 0.6 M PhOH under CO_2 saturation conditions. Conditions: 0.1 M $TBAPF_6$/DMF; glassy carbon disc working electrode, glassy carbon rod counter electrode, Ag/AgCl pseudoreference electrode; referenced to Fc^+/Fc internal standard; 100 mV/s scan rate. (**B**) Log-log plot from data obtained in **A** at –2.13 V vs. Fc^+/Fc.

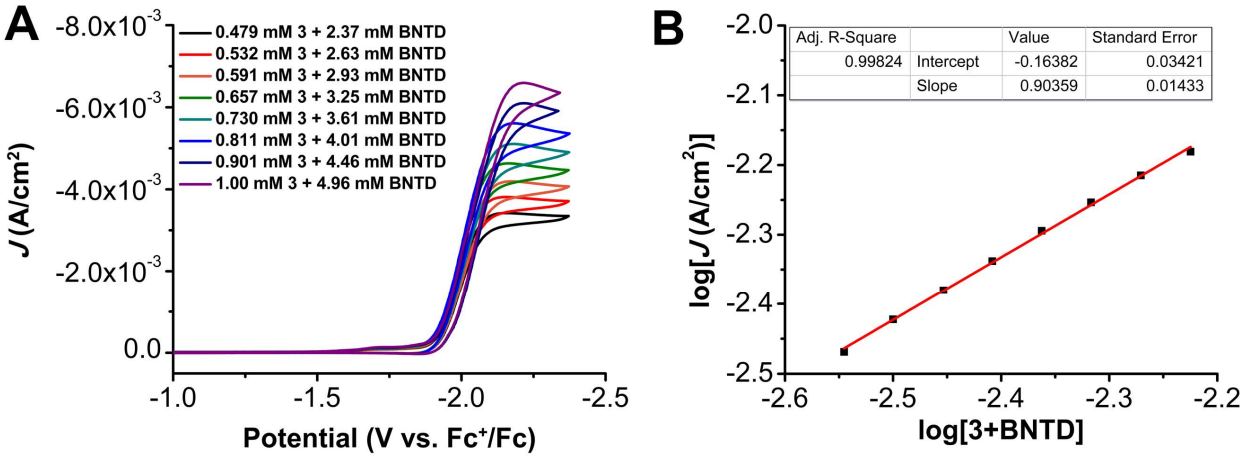

Figure S33. (**A**) CVs where the concentrations of Cr(^{tbu}dh^{tbu}bpy)Cl(H_2O) **3** and BNTD were varied at a fixed 1:5 ratio of **3**:BNTD with 0.5 M PhOH under CO_2 saturation conditions. Conditions: 0.1 M $TBAPF_6$/DMF; glassy carbon disc working electrode, glassy carbon rod counter electrode, Ag/AgCl pseudoreference electrode; referenced to Fc^+/Fc internal standard; 100 mV/s scan rate. (**B**) Log-log plot from data obtained in **A** at –2.22 V vs. Fc^+/Fc.

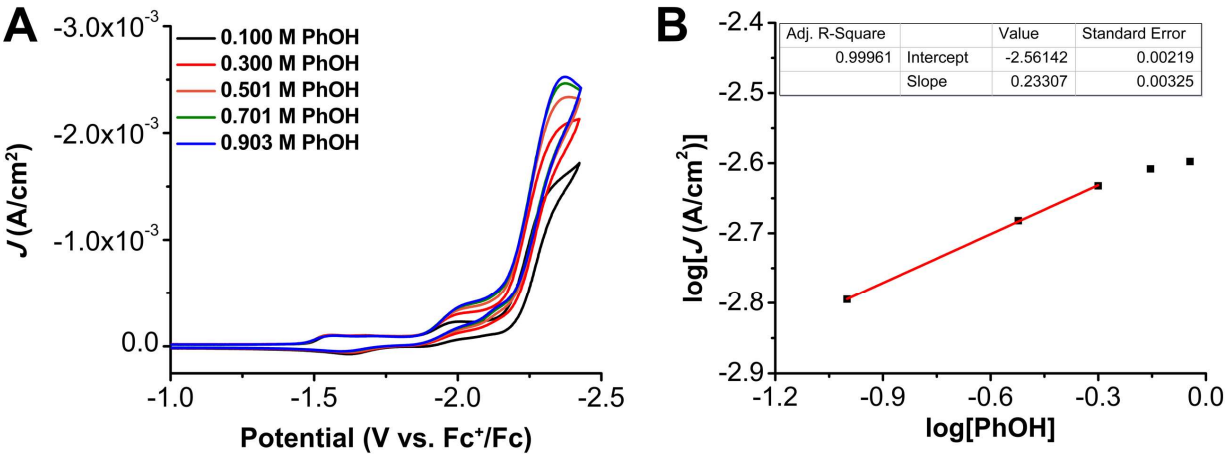

Figure S34. (**A**) CVs of PhOH at variable concentrations, obtained under CO_2 saturation with 1.0 mM Cr(^{tbu}dh^{Ph}phen)Cl(H_2O) **1** and 2.5 mM DBTD. Conditions: 0.1 M $TBAPF_6$/DMF; glassy carbon disc working electrode, glassy carbon rod counter electrode, Ag/AgCl pseudoreference electrode; referenced to Fc^+/Fc internal standard; 100 mV/s scan rate. (**B**) Log-log plot from data obtained in **A** at –2.37 V vs. Fc^+/Fc.

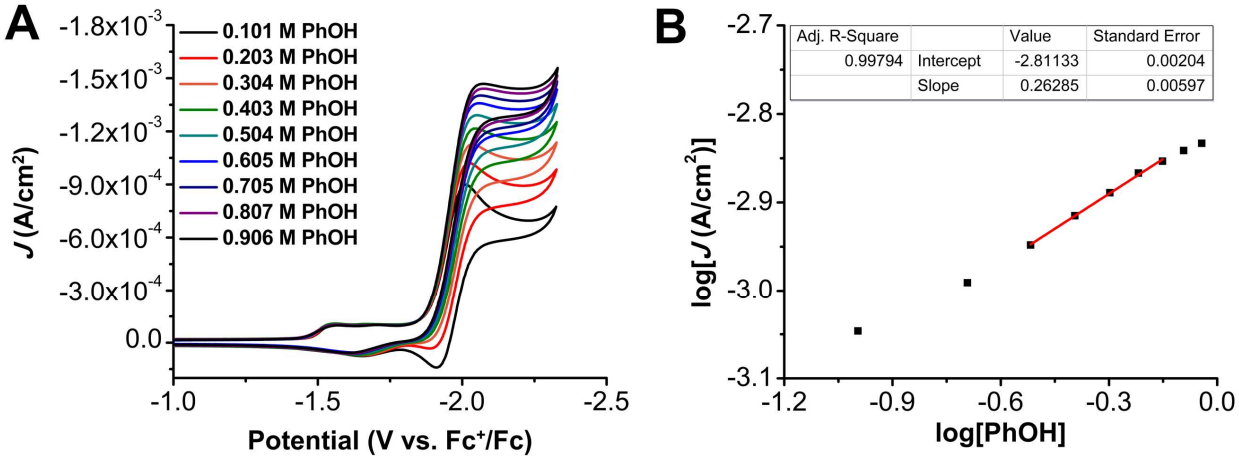

Figure S35. (**A**) CVs of PhOH at variable concentrations, obtained under CO_2 saturation with 1.0 mM Cr(^{tbu}dh^{Ph}phen)Cl(H_2O) **1** and 2.5 mM BNTD. Conditions: 0.1 M $TBAPF_6$/DMF; glassy carbon disc working electrode, glassy carbon rod counter electrode, Ag/AgCl pseudoreference electrode; referenced to Fc^+/Fc internal standard; 100 mV/s scan rate. (**B**) Log-log plot from data obtained in **A** at –2.07 V vs. Fc^+/Fc.

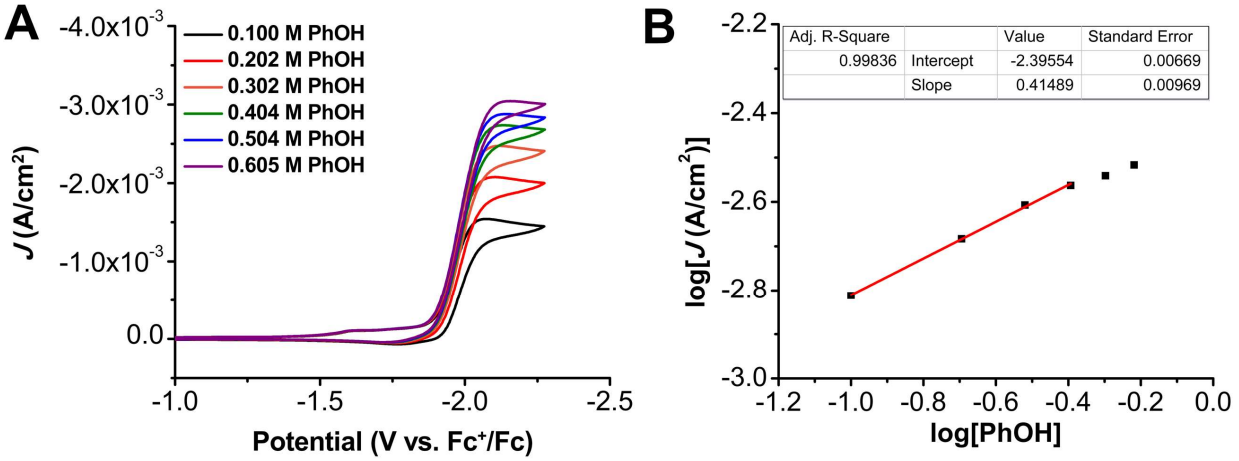

Figure S36. (**A**) CVs of PhOH at variable concentrations, obtained under CO_2 saturation with 1.0 mM Cr(^{tbu}dhphen)Cl(H_2O) **2** and 2.5 mM BNTD. Conditions: 0.1 M $TBAPF_6$/DMF; glassy carbon disc working electrode, glassy carbon rod counter electrode, Ag/AgCl pseudoreference electrode; referenced to Fc^+/Fc internal standard; 100 mV/s scan rate. (**B**) Log-log plot from data obtained in **A** at –2.12 V vs. Fc^+/Fc.

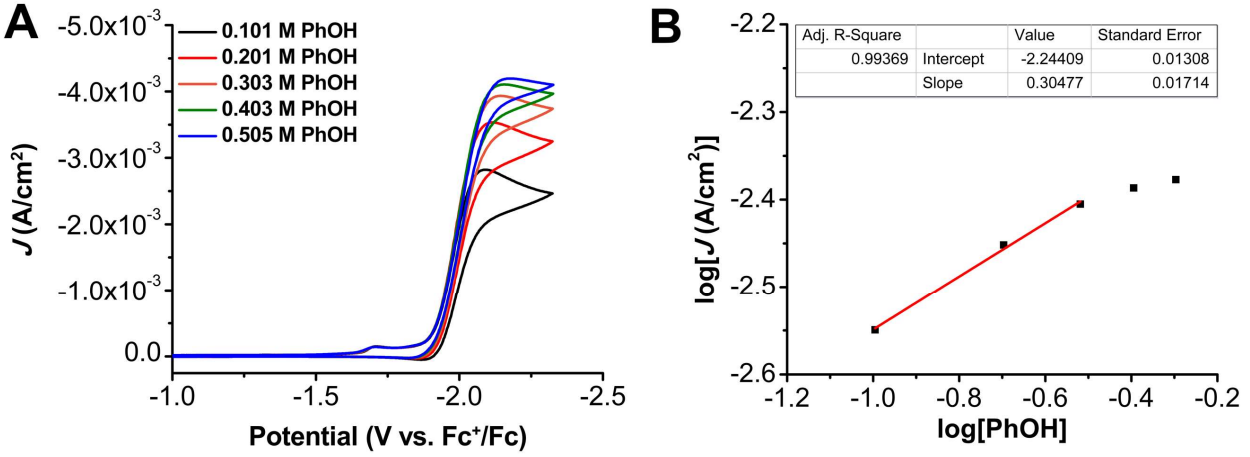

Figure S37. (**A**) CVs of PhOH at variable concentrations, obtained under CO_2 saturation with 1.0 mM Cr(^{tbu}dh^{tbu}bpy)Cl(H_2O) **3** and 2.5 mM BNTD. Conditions: 0.1 M $TBAPF_6$/DMF; glassy carbon disc working electrode, glassy carbon rod counter electrode, Ag/AgCl pseudoreference electrode; referenced to Fc^+/Fc internal standard; 100 mV/s scan rate. (**B**) Log-log plot from data obtained in **A** at –2.14 V vs. Fc^+/Fc.

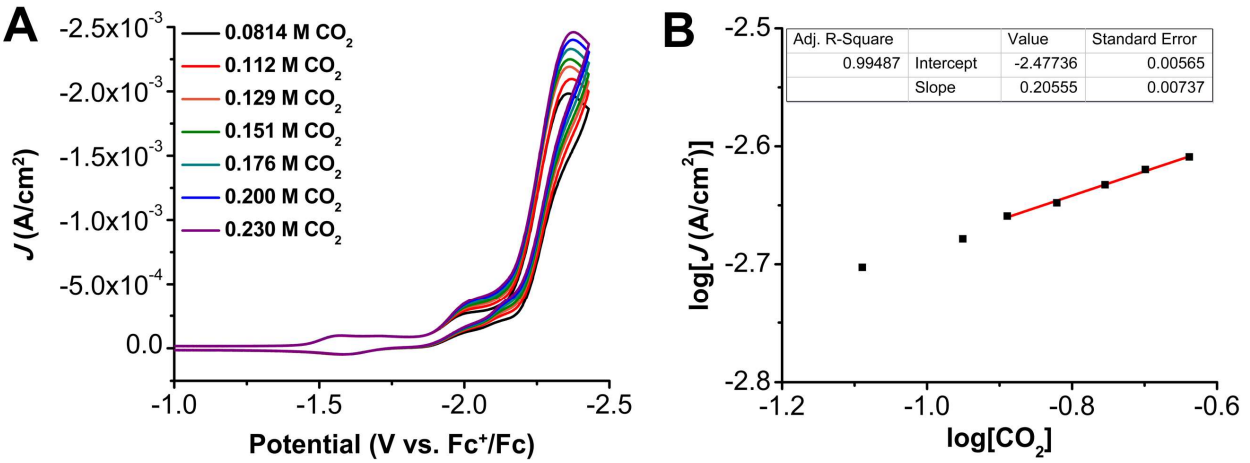

Figure S38. (**A**) CVs of 1.0 mM Cr(^{tbu}dh^{Ph}phen)Cl(H_2O) **1**, 2.5 mM DBTD, 0.9 M PhOH at varied CO_2 concentrations. Conditions: 0.1 M $TBAPF_6$/DMF; glassy carbon disc working electrode, glassy carbon rod counter electrode, Ag/AgCl pseudoreference electrode; referenced to Fc^+/Fc internal standard; 100 mV/s scan rate. (**B**) Log-log plot from data obtained in **A** at –2.36 V vs. Fc^+/Fc.

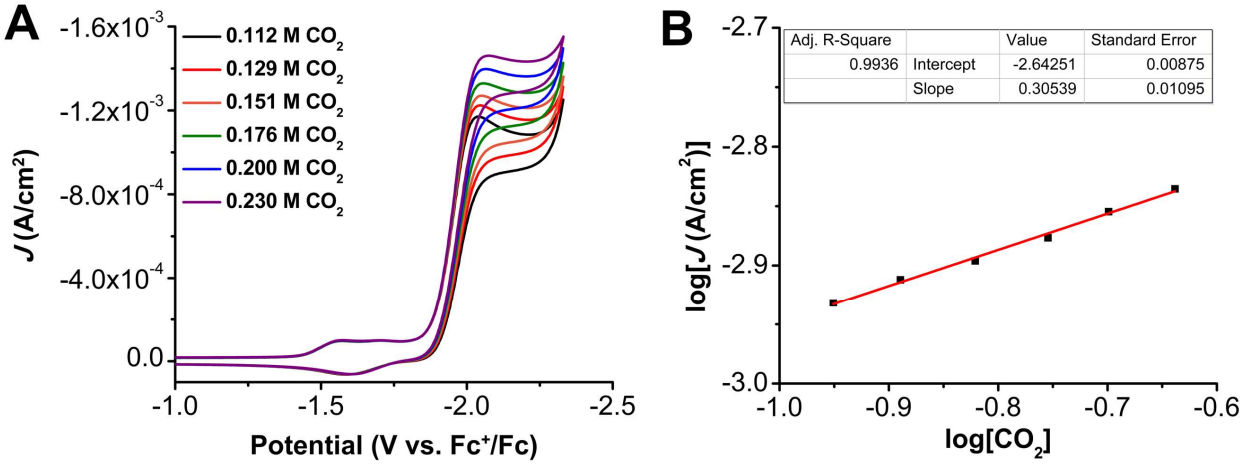

Figure S39. (**A**) CVs of 1.0 mM Cr(^{tbu}dh^{Ph}phen)Cl(H_2O) **1**, 2.5 mM BNTD, 0.9 M PhOH at varied CO_2 concentrations. Conditions: 0.1 M $TBAPF_6$/DMF; glassy carbon disc working electrode, glassy carbon rod counter electrode, Ag/AgCl pseudoreference electrode; referenced to Fc^+/Fc internal standard; 100 mV/s scan rate. (**B**) Log-log plot from data obtained in **A** at –2.07 V vs. Fc^+/Fc.

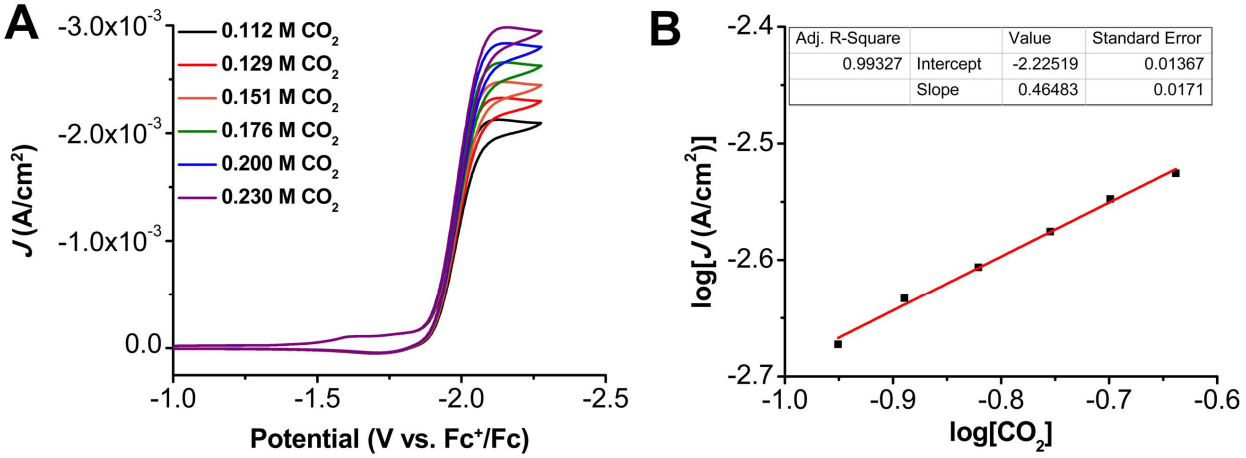

Figure S40. (**A**) CVs of 1.0 mM Cr(^{tbu}dhphen)Cl(H_2O) **2**, 2.5 mM BNTD, 0.6 M PhOH at varied CO_2 concentrations. Conditions: 0.1 M $TBAPF_6$/DMF; glassy carbon disc working electrode, glassy carbon rod counter electrode, Ag/AgCl pseudoreference electrode; referenced to Fc^+/Fc internal standard; 100 mV/s scan rate. (**B**) Log-log plot from data obtained in **A** at –2.14 V vs. Fc^+/Fc.

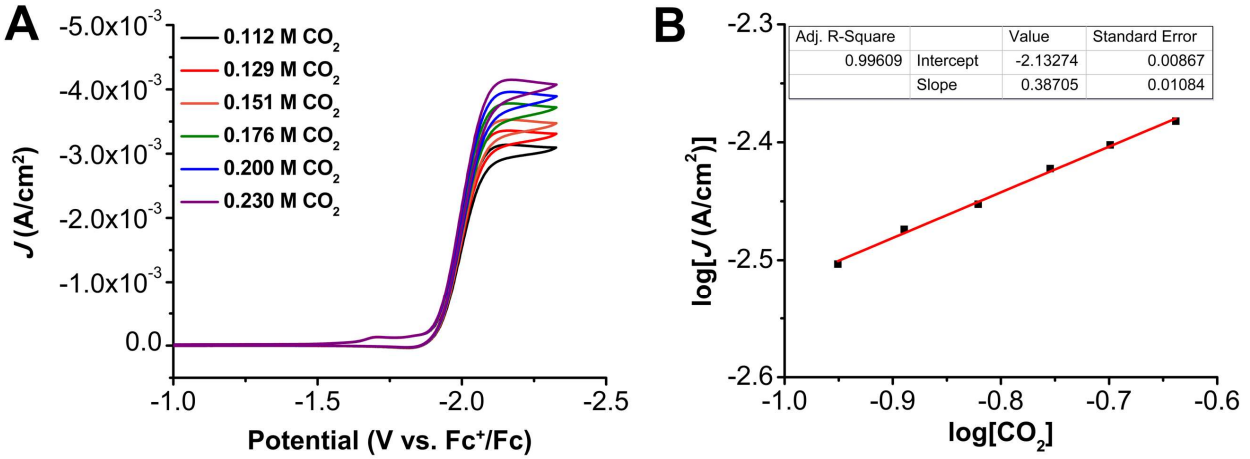

Figure S41. (**A**) CVs of 1.0 mM Cr(^{tbu}dh^{tbu}bpy)Cl(H_2O) **3**, 2.5 mM BNTD, 0.6 M PhOH at varied CO_2 concentrations. Conditions: 0.1 M $TBAPF_6$/DMF; glassy carbon disc working electrode, glassy carbon rod counter electrode, Ag/AgCl pseudoreference electrode; referenced to Fc^+/Fc internal standard; 100 mV/s scan rate. (**B**) Log-log plot from data obtained in **A** at –2.14 V vs. Fc^+/Fc.

CPE with Cr Catalysts and RMs

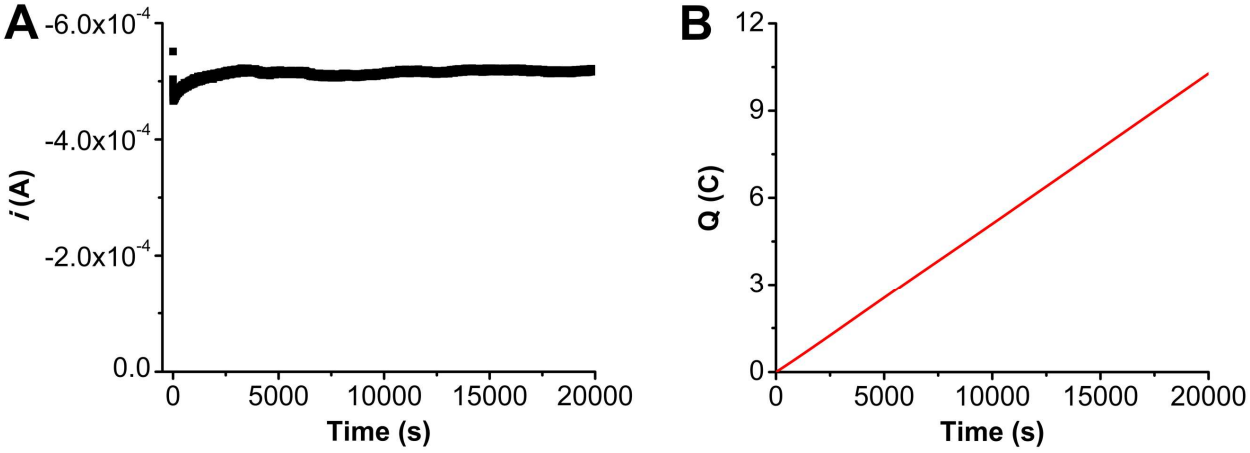

Figure S42. (**A**) Current versus time trace from CPE experiment for **1**+DBTD+PhOH. (**B**) Charge passed versus time for the CPE experiment shown in **A**. Conditions were 0.1 mM Cr(^{tbu}dh^{Ph}phen)Cl(H_2O) **1**, 0.5 mM DBTD, and 1.0 M PhOH under a CO_2 atmosphere at −2.30 V vs Fc^+/Fc in 0.1 M $TBAPF_6$/DMF; working electrode was a glassy carbon rod, counter electrode was a graphite rod, and the reference was a nonaqueous Ag/AgCl pseudoreference electrode; 0.075 M Fc was used as sacrificial oxidant.

Table S5. Results from CPE experiment in **Figure S42**, **1** + DBTD + PhOH.

Time (s)	Charge (coulombs)	Moles (e^-)	Moles of CO	FE_{CO}	Moles of H_2	FE_{H2}
20000*	10.3	1.07×10^{-4}	4.22×10^{-5}	79.2	1.05×10^{-5}	19.8
20000*	10.3	1.07×10^{-4}	4.02×10^{-5}	75.5	9.60×10^{-6}	18.0
20000*	10.3	1.07×10^{-4}	4.06×10^{-5}	76.1	9.32×10^{-6}	17.5

*indicates a series of injections carried out in triplicate upon completion of electrolysis

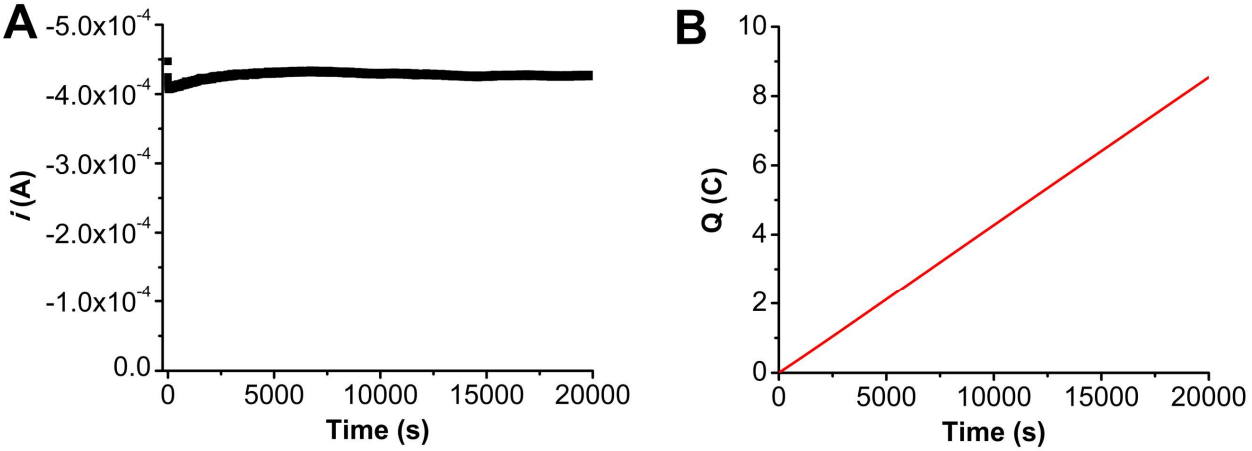

Figure S43. (**A**) Current versus time trace from CPE experiment for **1**+BNTD+PhOH. (**B**) Charge passed versus time for the CPE experiment shown in **A**. Conditions were 0.1 mM Cr(^{tbu}dh^{Ph}phen)Cl(H_2O) **1**, 0.5 mM BNTD, and 1.0 M PhOH under a CO_2 atmosphere at −2.20 V vs Fc^+/Fc in 0.1 M $TBAPF_6$/DMF; working electrode was a glassy carbon rod, counter electrode was a graphite rod, and the reference was a nonaqueous Ag/AgCl pseudoreference electrode; 0.075 M Fc was used as sacrificial oxidant.

Table S6. Results from CPE experiment in **Figure S43**, **1** + BNTD + PhOH.

Time (s)	Charge (coulombs)	Moles (e^-)	Moles of CO	FE_{CO}	Moles of H_2
13569	5.80	6.01×10^{-5}	2.80×10^{-5}	93.1	<LOQ
16528	7.06	7.32×10^{-5}	3.53×10^{-5}	96.6	<LOQ
19211	8.21	8.51×10^{-5}	4.22×10^{-5}	99.2	<LOQ
20791*	8.88	9.21×10^{-5}	4.53×10^{-5}	98.4	<LOQ
20791*	8.88	9.21×10^{-5}	4.52×10^{-5}	98.2	<LOQ
20791*	8.88	9.21×10^{-5}	4.52×10^{-5}	98.1	<LOQ

*indicates a series of injections carried out in triplicate upon completion of electrolysis

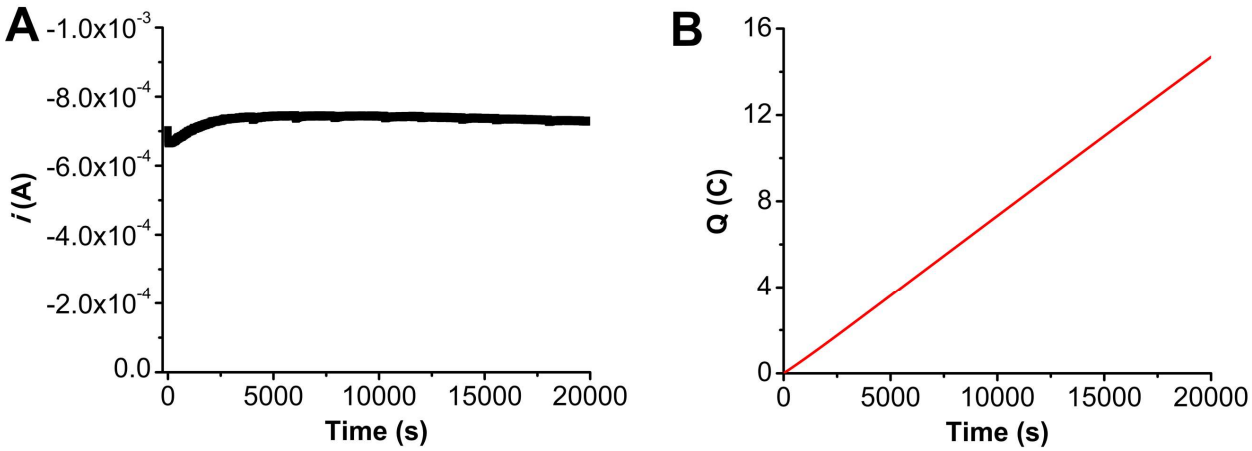

Figure S44. (**A**) Current versus time trace from CPE experiment for **2**+BNTD+PhOH. (**B**) Charge passed versus time for the CPE experiment shown in **A**. Conditions were 0.1 mM Cr(^{tbu}dhphen)Cl(H_2O) **2**, 0.5 mM BNTD, and 1.0 M PhOH under a CO_2 atmosphere at −2.20 V vs Fc^+/Fc in 0.1 M $TBAPF_6$/DMF; working electrode was a glassy carbon rod, counter electrode was a graphite rod, and the reference was a nonaqueous Ag/AgCl pseudoreference electrode; 0.075 M Fc was used as sacrificial oxidant.

Table S7. Results from CPE experiment in **Figure S44**, **2** + BNTD + PhOH.

Time (s)	Charge (coulombs)	Moles (e^-)	Moles of CO	FE_{CO}
11982	8.79	9.11×10^{-5}	4.33×10^{-5}	93.4
13926	10.2	1.06×10^{-4}	5.25×10^{-5}	95.1
15525	11.4	1.18×10^{-4}	6.30×10^{-5}	107
18025	13.2	1.37×10^{-4}	7.01×10^{-5}	102
20000*	14.7	1.52×10^{-4}	7.91×10^{-5}	104
20000*	14.7	1.52×10^{-4}	8.19×10^{-5}	108
20000*	14.7	1.52×10^{-4}	8.27×10^{-5}	109

*indicates a series of injections carried out in triplicate upon completion of electrolysis

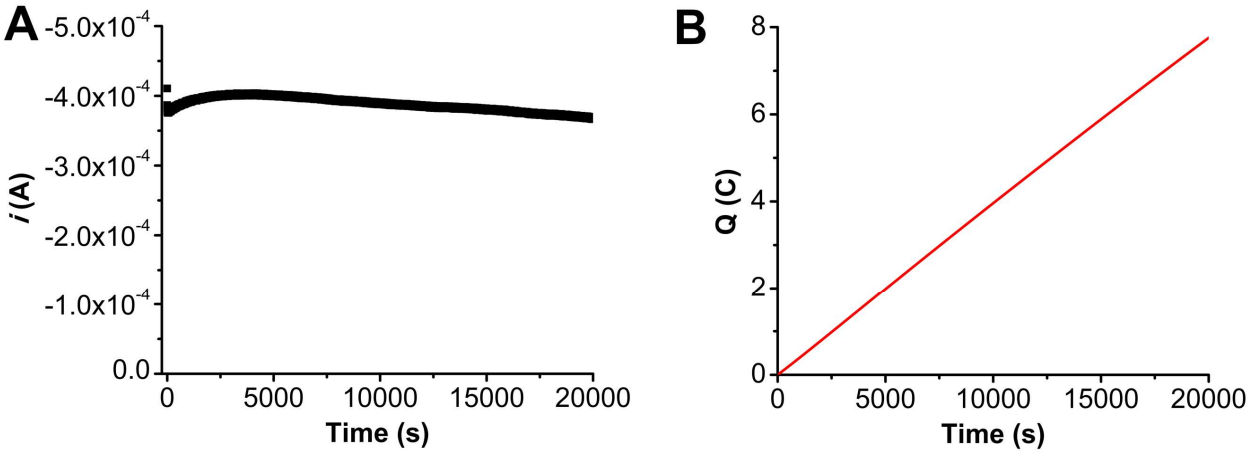

Figure S45. (**A**) Current versus time trace from CPE experiment for **3**+BNTD+PhOH. (**B**) Charge passed versus time for the CPE experiment shown in **A**. Conditions were 0.1 mM Cr(^{tbu}dh^{tbu}bpy)Cl(H_2O) **3**, 0.5 mM BNTD, and 0.12 M PhOH under a CO_2 atmosphere at −2.20 V vs Fc^+/Fc in 0.1 M $TBAPF_6$/DMF; working electrode was a glassy carbon rod, counter electrode was a graphite rod, and the reference was a nonaqueous Ag/AgCl pseudoreference electrode; 0.075 M Fc was used as sacrificial oxidant.

Table S8. Results from CPE experiment in **Figure S45**, **3** + BNTD + PhOH.

Time (s)	Charge (coulombs)	Moles (e^-)	Moles of CO	FE_{CO}
20000*	7.76	8.04×10^{-5}	4.16×10^{-5}	103
20000*	7.76	8.04×10^{-5}	3.99×10^{-5}	99.2
20000*	7.76	8.04×10^{-5}	3.92×10^{-5}	97.5

*indicates a series of injections carried out in triplicate upon completion of electrolysis

References:

1. S. L. Hooe, J. M. Dressel, D. A. Dickie and C. W. Machan, *ACS Catal.*, 2020, **10**, 1146-1151.
2. M. L. Pegis, C. F. Wise, D. J. Martin and J. M. Mayer, *Chem. Rev.*, 2018, **118**, 2340-2391.
3. M. L. Pegis, J. A. S. Roberts, D. J. Wasylenko, E. A. Mader, A. M. Appel and J. M. Mayer, *Inorg. Chem.*, 2015, **54**, 11883-11888.
4. A. G. Reid, M. E. Moberg, C. A. Koellner, J. J. Moreno, S. L. Hooe, K. R. Baugh, D. A. Dickie and C. W. Machan, *Organometallics*, 2023, **42**, 1139-1148.
5. A. G. Reid, J. J. Moreno, S. H. Hooe, K. R. Baugh, I. H. Thomas, D. A. Dickie and C. W. Machan, *Chem. Sci.*, 2022, **13**, 9595-9606.
6. M. F. Nielsen, O. Hammerich, F. Rise, A. Gogoll, K. Undheim, D. N. Wang and S. B. Christensen, *Acta. Chem. Scan.*, 1992, **46**, 883-896.
7. S. Roy, B. Sharma, J. Pécaut, P. Simon, M. Fontecave, P. D. Tran, E. Derat and V. Artero, *J. Am. Chem. Soc.*, 2017, **139**, 3685-3696.
8. Y. Matsubara, *ACS Energy Lett.*, 2019, **4**, 1999-2004.
9. C. Costentin, S. Drouet, M. Robert and J.-M. Savéant, *J. Am. Chem. Soc.*, 2012, **134**, 11235-11242.
10. C. Costentin, S. Drouet, M. Robert and J.-M. Savéant, *J. Am. Chem. Soc.*, 2012, **134**, 19949-19950.
11. C. Cometto, L. Chen, P.-K. Lo, Z. Guo, K.-C. Lau, E. Anxolabéhère-Mallart, C. Fave, T.-C. Lau and M. Robert, *ACS Catal.*, 2018, **8**, 3411-3417.
12. J. E. Baur, in *Handbook of Electrochemistry*, ed. C. G. Zoski, Elsevier, 2007, DOI: DOI 10.1016/B978-044451958-0.50000-8, pp. 829-848.
13. Bruker, *Journal*, 2012.
14. L. Krause, R. Herbst-Irmer, G. M. Sheldrick and D. Stalke, *J. Appl. Crystallogr.*, 2015, **48**, 3-10.
15. G. Sheldrick, *Acta Cryst.*, 2015, **71**, 3-8.
16. O. V. Dolomanov, L. J. Bourhis, R. J. Gildea, J. A. K. Howard and H. Puschmann, *J. Appl. Cryst.*, 2009, **42**, 339-341.
17. T. Marshall-Roth, N. J. Libretto, A. T. Wrobel, K. J. Anderton, M. L. Pegis, N. D. Ricke, T. V. Voorhis, J. T. Miller and Y. Surendranath, *Nat. Commun.*, 2020, **11**, 5283.
18. D. H. Grant, *J. Chem. Educ.*, 1995, **72**, 39.
19. G. A. Bain and J. F. Berry, *J. Chem. Educ.*, 2008, **85**, 532-536.
20. A. J. Sathrum and C. P. Kubiak, *J. Phys. Chem. Lett.*, 2011, **2**, 2372-2379.